Portland State University

PDXScholar

1998

Spectroscopy of Charge-Coupled Devices

Lars Mündermann
Portland State University

Follow this and additional works at: https://pdxscholar.library.pdx.edu/open_access_etds

 Part of the Physics Commons

Let us know how access to this document benefits you.

THESIS APPROVAL

The abstract and thesis of Lars Mündermann for the Master of Science in Physics were presented August 4, 1998, and accepted by the thesis committee and the department.
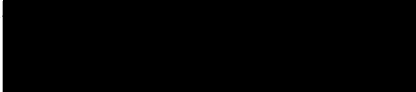
COMMITTEE APPROVALS:
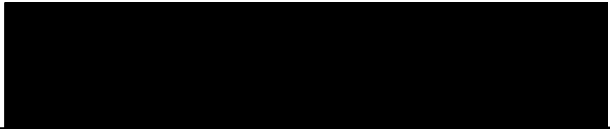
Erik Bodegom, Chair

Jon Abramson

Lee Casperson
Representative of the Office of Graduate Studies

DEPARTMENT APPROVAL:

Erik Bodegom, Chair
Department of Physics

ABSTRACT

An abstract of the thesis of Lars Mündermann for the Master of Science in Physics presented August 4, 1998.

Title: Spectroscopy of Charge-Coupled Devices

A systematic study of persistent, or residual, images occurring in CCD imagers and a systematic study of dark current generation in CCD imagers are presented. These effects are a source of unwanted signal in frames, and should be considered where very exact, low light-level signal processing is necessary. For both studies explanatory models and statistical analysis techniques have been developed which enable the derivation of the densities and the characteristic energies. Furthermore the importance of understanding these phenomena in the context of today's low light-level imaging is discussed.

Impurity sites are found to be responsible for residual images. Photo-electrons are trapped at impurity sites and thermally released over time. From the analysis the initial number of loaded traps and a trapping energy of 0.48 eV are found. In addition, the optical excitation rate and the maximum number of available trapping sites per pixel are derived.

For the systematic study of the dark current, a quantization of the dark current and the existence of different pixel groups in a CCD imager are shown. The pixels are split into different groups (negative pixels, non-linear pixels,

normal pixels, hot pixels) and models are developed to explain the different sources of dark current. For each group an explanatory model and a statistical analysis technique have been developed which enables the derivation of the densities and the characteristic energies responsible for these effects. For normal pixels the diffusion current is found to cause the dark current. Furthermore, for hot pixels and non-linear pixels an interface state generated component of the dark current is found in addition to diffusion current.

SPECTROSCOPY OF CHARGE-COUPLED DEVICES

by

LARS MÜNDERMANN

A thesis submitted in partial fulfillment of the
requirements for the degree of

MASTER OF SCIENCE
in
PHYSICS

Portland State University
1998

für meine Eltern

Table of Contents

List of Tables

List of Figures

1 Introduction

Charge-Coupled Devices (CCDs) were invented by Boyle and Smith of Bell Laboratories in 1970.[1,2] They were initially designed as memory to replace magnetic bubble devices. A packet of charge (electrons (e-) or holes (h+)) stored in the depletion region of a Metal Oxide Semiconductor (MOS) capacitor represents one bit of information in a CCD. By placing the MOS capacitors very close together these charges can be moved by manipulating the voltage on the gates on each capacitor. This can be done by forcing the charge to spill from one capacitor to the next.[3] Finally a charge detection amplifier detects the presence of the charge packet.

It turned out that the CCDs were sensitive to light. Photons were able to generate a charge packet in the depletion region of the MOS capacitor. CCDs are now used solely as light detectors and offer several benefits in the detection of light compared to photographic film, i.e. the sensitivity is much higher than film.

The CCD is a serial device where charge packets are read one at a time. The process of moving the charge from one gate to another gives rise to the name charge-coupled device.

2 Theoretical Background

2.1 CCD Theory and Operation

To generate an image a CCD must perform charge generation, charge collection, charge transfer, and charge detection. Charge generation relies on the photoelectric effect – when photons penetrate material, electrons can be excited to the conduction band. These photo-excited electrons are collected in the nearest discrete collecting sites or pixels. The collection sites are defined by an array of electrodes, called gates, formed on the CCD. Charge transfer is accomplished by manipulating the voltage on the gates in a systematic way so the signal electrons move down the vertical registers from one pixel to the next. The final step is when individual charge packets are converted to an output voltage.

2.2 Photoelectric Effect

The energy gap in silicon between the valence and conduction band is approximately 1.1 eV.[4] Energetic particles falling on and penetrating a semiconductor substrate can transfer a part of their energy to the substrate. This energy transfer can take place by the generation of electron-hole (e-h) pairs. If the energy content of the particles is high enough, electrons can be released from the valence band and swept into the conduction band. This action reduces the energy of the incoming particle by an amount equal to the energy difference

between the conduction and the valence bands, i.e. the band gap. As a consequence, the energy of the particle has to be higher than the band gap to generate an electron-hole pair.

2.3 MOS Capacitor and Depletion

The electron-hole pairs have to be separated after the generation of the charge carriers in the bulk. The easiest method is to use an electrical field for trapping the electrons and draining the holes to the substrate.

The basis for the CCD is a Metal-Oxide-Semiconductor (MOS) capacitor. There are two types of MOS capacitor structures: surface channel and buried channel. Because of its major advantages, all CCDs today utilize the buried channel structure. Typically, the device is built on a p-type epitaxial silicon substrate. An n-type region (~1 µm thick) is formed on the surface. Next, a thin silicon dioxide layer is grown (~0.1 µm thick) followed by a metal or heavily doped polycrystalline silicon layer. The latter layer forms the electrode or gate and completes the capacitor. Figure 1 shows the cross section of a typical buried channel structure.

The potential wells shown for two different gate voltages illustrate how photo-electrons are collected in the n-type region. The charge packets are confined to a channel that lies beneath the surface – "buried" in the silicon.
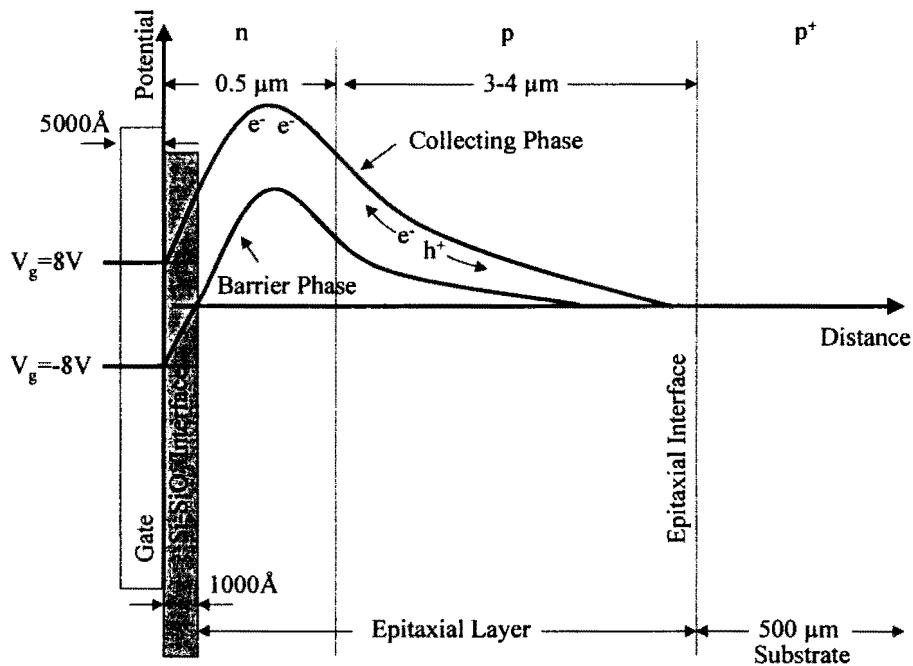
Fig. 1   Buried channel Metal-Oxide-Semiconductor and the typical potential well for two different gate voltages (V_g=8V and V_g=-8V).

2.4   CCD Pixel

The CCD is composed of an array of closely spaced MOS capacitors. The simplest format for a single CCD pixel is three gates oriented perpendicular to two channel-stop regions. These regions separate the individual rows. Between the channel stop regions lies the buried channel. If the potential on the middle electrode is more positive than that applied to either of the other two gates, a local potential energy minimum will be formed under the middle gate. Electrons created within the potential minimum will be collected there. Figure 2 shows the simplest format for a single pixel.
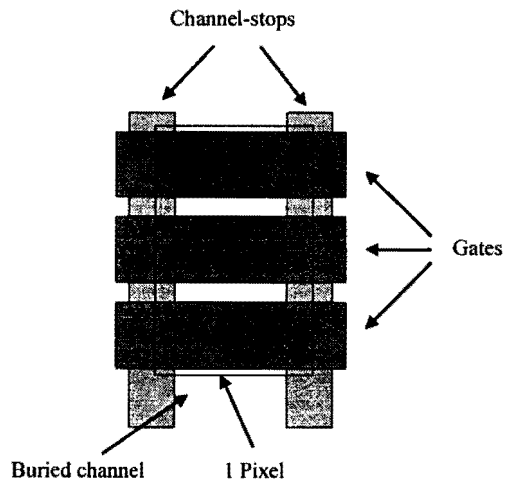
Fig. 2   Simplest format for a single pixel.

2.5   Charge Transfer Process and Efficiency

The quantity of charge accumulated beneath the integrating gate has to be read out. This involves moving the packet from the site of collection through other pixels to a charge detecting amplifier located at the end of the linear pixel array.

The charge transfer efficiency (CTE) is a measure of the ability of the device to transfer charge from one pixel to the next. Typically, for well-made buried channel devices, the CTE is between 99.999% and 99.9999%. CTE is mainly influenced by three factors related to electron traps: process traps, bulk traps, and radiation traps.

2.5.1 Processed Induced Traps

Processed induced traps can be classified into two categories: those that are uniformly distributed along the signal channel and cause a global CTE effect (these are referred to as spurious potential pockets), and those that are randomly distributed and isolated to individual pixels (these are referred to simply as localized traps).

Spurious potential pockets is a term used to describe loss of charge during charge transfer due to improper potential well shape and/or depth beneath the pixel.

Localized traps are usually confined to single pixels. These traps are capable of capturing a wide range of charge, from a few electrons to several thousands electrons. Detailed tests show that they are localized in a single level of poly-silicon within a pixel.[5] Defects like this affect CTE on a local, random level.

2.5.2 Bulk Traps

Bulk traps are due to deep-level metallic impurities (such as gold, iron etc.) or lattice defects associated with the silicon material on which the CCD is built. Bulk traps that happen to lie within the charge transfer channel will trap charge typically involving a single electron. Bulk traps are generally not a problem for CTE performance since modern starting wafers and processes used to fabricate the CCD have been improved enormously. However, bulk traps

determine the ultimate CTE that can be achieved by the CCD (i.e., CTE performance is bulk state limited).

2.5.3 *Radiation Induced Traps*

Radiation traps are induced in the signal channel by energetic particles and photons (e.g. protons, electrons, neutrons, heavy ions, gamma rays, etc.) that displace silicon atoms from the lattice structure. Silicon vacancies created by incident radiation are unstable and typically migrate to favorable positions in the lattice. Usually vacancies become trapped near impurity atoms due to the stress imposed by the impurities on the lattice.

2.6 Quantum Efficiency

The quantum efficiency (QE) is a measure of the efficiency with which incident photons are detected. The QE is the ratio of the number of detected electrons divided by the product of the number of incident photons multiplied by the number of electrons each photon can be expected to generate.

There are two types of CCD imager: front-illuminated and back-illuminated devices. These devices differ only slightly in their fabrication.

A front-illuminated CCD imager is exposed from the gate side. Therefore incident photons must pass through a passivation layer as well as through the gate structure in order to generate signal electrons.

A back-illuminated device is mounted with the gate structure against a rigid substrate. The incident photons do not have to pass through the front

surface electrodes and layers. In addition, an enhancement layer is added to the back surface to create an electric field that forces photo-generated electrons toward the potential well under the gates.

Hence, front-illuminated devices generally have a lower QE.

2.7 Dark Current Noise

One important source generated internally in the CCD is dark current. Dark current occurs due to thermally generated electrons within the device and represents an inherent limitation on read performance due to the dark shot noise that is produced. Thermally generated charge is governed by Poisson statistics.

For CCD imagers there are three main sources of dark current within the device. These are 1) thermal generation and diffusion in the neutral bulk, 2) thermal generation in the depletion region, and 3) thermal generation due to surface states at the Si-SiO$_2$ interface. Surface dark current is two to three orders of magnitude greater than dark current generated by the bulk of the CCD.[6]

Dark current generation at the Si-SiO$_2$ interface depends on two factors, namely the density of interface states and the density of free carriers (holes or electrons) that populate the interface. Electrons that thermally "hop" from the valence band to an interface state and then to the conduction band will be collected in the potential well.

2.8 Inversion

In 1980 Saks introduced a technique to reduce the dark current generation at the Si-SiO$_2$ interface.[7] The technique employed was to bias the interface of the buried channel imager into inversion, thereby suppressing generation by interface states. When a gate (phase) is driven negatively such that the surface and the substrate potential become equal (see barrier phase in figure 1), the n-channel at the Si-SiO$_2$ interface inverts. In this case, holes from the channel-stops are attracted and collect at the surface. Free carriers will fill the interface state inhibiting the hopping conduction mechanism, and substantially reduce dark current generation to the bulk rate level.

Non-inverted CCDs deplete the interface of free carriers, maximizing surface dark current generation. Under depleted conditions, dark current generation is solely a function of the density of interface states at the Si-SiO$_2$ interface.

Under inversion some of these holes become trapped at the Si-SiO$_2$ interface. When the gate voltage is switched to transfer charge, trapped holes are released with sufficient energy to create electron-hole pairs. These spurious electrons are then collected in the nearest potential well (referred to as spurious charge). Spurious charge generation can usually be reduced to negligible levels.

2.9 Multi-pinned phase

Multi-pinned phase (MPP) CCDs can operate totally inverted, thus achieving ultra-low dark current generation rates. However, once holes are present at the interface under all gates, no difference in channel potential remains for separating charge packets. An additional p-type implant is provided under one of these three phases, causing a "profiled" CCD channel potential such that charge packets can be kept separated.[8]

2.10 Residual Images

There are two distinct forms of residual images exhibited in CCDs: surface residual image (SRI) and residual bulk image (RBI).[9]

2.10.1 Surface Residual Image

A surface residual image occurs when the CCD is overexposed to light or when the buried channel becomes undepleted. Under either of these conditions, electrons are trapped at the frontside $Si-SiO_2$ interface. The trapped charge is released slowly and is seen as a residual image in subsequent long dark integration periods (the emission time constants of interface traps increase exponentially with decreasing temperature). SRI can be completely eliminated when the CCD is driven into inversion. In that case trapped charge under a phase instantly recombines with holes.

2.10.2 Residual Bulk Image

A residual bulk image is associated with trapping centers at the epitaxial interface. RBI is predominantly seen at wavelengths greater than 7000Å where the photons penetrate beyond the depletion region to the epitaxial interface and substrate regions of the CCD. For wavelengths below 6000Å it is difficult to detect RBI because most photons at this wavelengths do not reach the interface. RBI does not appear in back-illuminated CCDs because the epitaxial interface is eliminated.

3 Instruments and Methods

3.1 Instruments

3.1.1 Camera System

An AX-2 CCD camera system manufactured by Axiom Research Inc., Tucson, Arizona was used for all experiments.[10] The camera head is a S-type model with a built-in CCD detector and a heat sink on the backside. The frontside connects to lenses and other instruments through a standard T-thread lens mount.

3.1.2 Detector

The detector, a Kodak KAF 1600-2, is a frontside-illuminated three-phase CCD with a pixel area of 14.0 x 9.3 mm. It is divided into 1536 imaging columns and 1024 imaging rows with 9 by 9 μm pixels. According to the specifications, the detector has a well depth of 85,000 electrons, a dynamic range of > 76db, a read noise of 13-20 electrons, a dark count of 50 electrons/second/pixel at 25° Celsius and a doubling temperature of 5-6° Celsius. A 16 bit analog-digital (A/D) converter is used to digitize the charge.

3.1.3 Thermal Control System

The camera combines active and passive thermal control designs to achieve cooling capacity and temperature stability. The active part of the

system uses a one-stage thermoelectric cooler with closed-loop stabilization through the Temperature Control Unit (TCU). The TCU continuously monitors the CCD sensor temperature and makes corrections to keep it stable within approximately 0.1°C. The maximum cooling capacity is 38°C below ambient temperature.

3.1.4 Lab Setup

The camera was connected to a computer with a Pentium processor (120 MHz), 16 MBytes memory and a 1.6 GBytes hard disk. This was sufficient to work with the camera quickly and efficiently. A 28-200 Tokina SZ-X 282 lens was connected to the camera. For flat-fielding, a video screen and two lamps were used. Additionally, white paper was fixed in front of the lens in order to get an uniformly illuminated sensor. All data were collected with this setup.

3.2 Methods

In order to increase the processing speed and to save memory, sub-frames were taken instead of full frames. For the experiments three different kinds of frames were taken: bias, dark, and flat frames.

3.2.1 Bias frame

A bias frame is a calibration image that shows the electronic bias offset inherent to every image obtained with a CCD sensor. The raw bias count (B) can be split into a noise free bias offset (O) and a bias structure (S). The total

bias count varies from pixel to pixel, the bias offset is a constant, and the bias structure again varies from pixel to pixel.

$$B = O + S$$

Typically, the bias level drifts up and down with small temperature changes in the CCD camera system. Thus, the best estimate is given by measuring the bias immediately after an image is taken.[11]

3.2.2 Dark frame

A dark frame is a calibration image that shows the amount of dark count produced by the CCD sensor in a given amount of time. Dark count is generally heavily dependent on exposure time and temperature. The raw dark count (D_R) can be split into a dark count (D) and a bias count (B).

$$D_R = D + B$$

3.2.3 Flat frame

A flat frame is a calibration image that shows the variations in response to light (quantum efficiency) across the CCD detector. The raw flat count (F_R) can be split into a flat count (F), dark count (D), and bias count (B).

$$F_R = F + D + B$$

3.2.4   Calibrated Images

To determine the real flat frame a dark frame must be subtracted from the flat frame. To determine a real dark frame a bias frame has to be subtracted from the dark frame. This can be done in two possible ways: 1) a master dark frame for a certain temperature and exposure time can be calculated and subtracted from each flat frame or 2) a corresponding dark frame taken shortly after each flat frame can be subtracted from the flat frame. Because of temperature drifts in the bias frame, the second method was used for all experiments. Dark frames were determined by subtracting single bias frames from the dark frames; flat frames were determined by subtracting single dark frames from the flat frames.

For a flat field the raw image signal or count – obtained in the readout of each pixel after an exposure – is an imperfect mapping of the incident light (the true signal). In addition to the true signal, one must consider the effects of thermally generated electrons (dark count (D)), electrons generated by the bias/readout voltage (bias count, (B)), the response function of the individual pixels, and optical effects such as dust shadowing or vignetting. The dark count is dependent on temperature and exposure time and can be measured for a given image by taking an equivalent exposure with the shutter closed. The bias count is introduced with each readout and can be measured by reading out a zero-second exposure. The response function of the pixels-plus-optics is a multiplicative effect (F) and can be determined by taking a flat field exposure

of a uniformly illuminated flat field. Understanding these effects, one can remove them from the raw image signal in order to obtain a corrected, or calibrated, signal.

The raw, or measured, signal ($S_{measured}$) as the real signal convoluted with the above effects can be written as

$$S_{measured} = F\,S_{real} + D + B$$

To get at the "true" signal, we deconvolute these effects to obtain a calibrated image or signal (S_{cal}):

$$S_{cal} = \frac{S_{measured} - D - B}{F}$$

This sort of image-processing, or calibrating, is routinely done for CCD images, and represents the best form of image processing one can do given these sources of extraneous signal. Ideally, the calibrated image S_{cal} would be equal to the desired "true" image but for noise fluctuations in $S_{measured}$, D, B, and F.

4 Systematic study of ghosting

4.1 Introduction

As discussed earlier, a CCD contains different traps. In the context of today's low-level-light imaging it is very important to understand and to determine these phenomena. Different groups have developed hardware and software methods to determine traps.[12,13]

This study contains a systematic study of another source of extraneous signal: electrons generated in previous exposures and trapped at impurity sites. These electrons are released in subsequent exposures and appear as residual images, or "ghosts". An analysis technique is described that enables the derivation of trap densities and characteristic energies responsible for these effects.

4.2 Observation of ghosting

The phenomena of ghost, or lingering, images is illustrated in figures 3 and 4. Figure 4 is a dark frame taken shortly after a normal exposure containing a reflected laser spot. An image of the laser spot was observed in the subsequent dark frame, lingering above the normal dark count.

Given a charge transfer efficiency of >99.999%, one would expect the possibility of 1 electron in 100,000 to be left behind after readout and each subsequent "flush". With a maximum exposure count of less than 32k, no

noticeable residual effects due to imperfect charge transfer should be expected. Furthermore, any effect due to imperfect charge transfer would leave a vertical streaked "ghost" as it sequentially transfers the charge packet from the exposure down through successive rows of pixels – something which can not be observed.
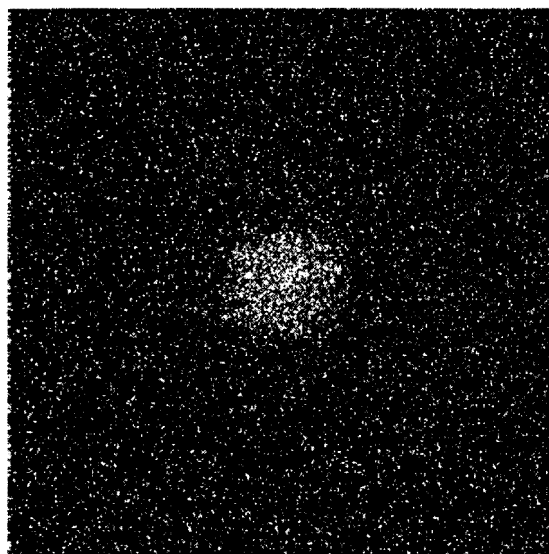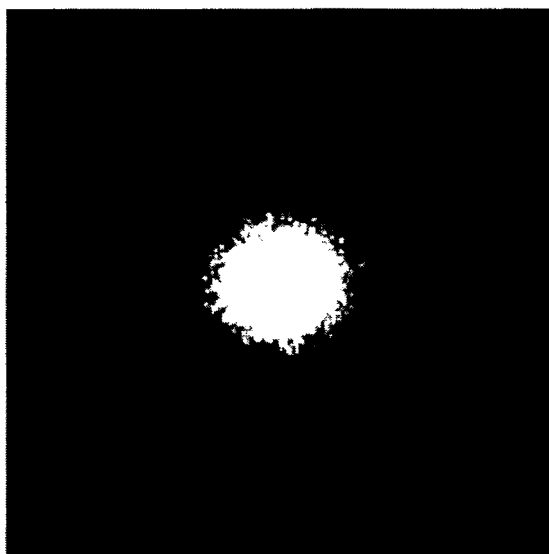
Fig. 3   Flat field of a laser spot (670 nm). **Fig. 4**   Dark image twenty seconds after the
The pixels were loaded well beyond full well.   end of the flat field exposure.

This "ghosting" phenomenon has been reported previously, but with only brief speculation as to its nature and cause. Epperson et al.[14] reported the observation of such "latent" images in front-illuminated CCDs exposed to long-wavelength light and attributed them to photo-electrons trapped at impurity sites at the epitaxy/substrate junction, and thermally released over time. Janesick et al.[15] reported the observation of two different types of residual

images – surface residual images which were observed when the pixels were loaded well beyond full-well, and residual bulk images seen predominantly at longer wavelength exposure (deep penetration depths). They noted that SRI can be neutralized by appropriate voltage clocking of the CCD gates (inversion) whereas RBI cannot.

The latent images studied here are immune to clocking voltages and appear well below full-well exposure. In accordance with previous studies then, these images are ascribed to trapping sites in the "bulk", or epitaxy/substrate interface. A detailed, quantitative analysis of this effect is described, along with an explanatory model.

The Kodak CCD imager operates in MPP, therefore SRI should not be seen. Figure 3 shows a 300x300 pixel sub-frame of the CCD imager. This area has been divided into 9 equal 100x100 segments. Figure 5 shows the average dark count as a function of time for each segment. The first three dark count data points were taken before the center segment was illuminated and the last ten dark count data points were taken immediately after the center segment was illuminated. The lines in this figure simply connect the dark counts and help to visually accentuate the residual bulk image effect.

The graphs in figure 5 show that only the center segment has a higher dark count after the flat field exposure. The segments below, above, to the left and right do not show any characteristic change in the dark count. Thus, there is no evidence of streaking.
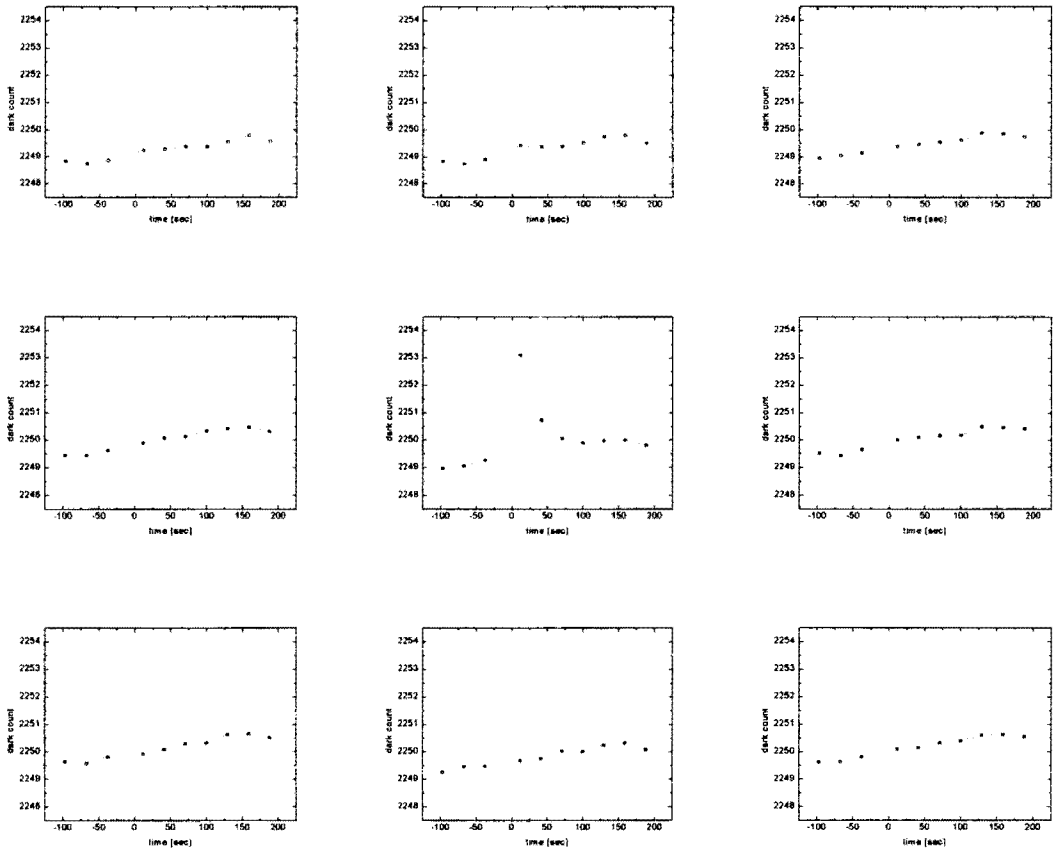
Fig. 5   Dark count as a function of time for nine equal segments of figure 3. Only the illuminated center segment shows a higher dark count after the flat field exposure.

4.3   Experimental

To understand the nature of these "ghosts", a systematic study of their time and temperature dependence was performed. The imager examined was a Kodak KAF 1600-2 sensor. In order to increase the speed of processing and save memory a 700x200 pixel sub-frame was used.

The procedures for an experiment at a constant temperature, a constant flat exposure time, and a constant light-intensity condition were as follows.

Five sets of a dark frame (D_i, i=1,2,..,5) and its associated bias frame (B_i, i=1,2,..,5) were taken. Then the CCD imager was exposed to a flat field for a certain exposure time and a certain light-intensity condition, loading the pixels uniformly and well below saturation. Immediately after the flat field, a series of ten dark (D_i, i=6,7,..,15) and bias frames (B_i, i=6,7,..,15) were taken.

The first five dark and five bias frames were used to calculate the normal dark and normal bias count. For all calculations the average count over all pixels in the corresponding sub-frame was used. The average dark count ($D_{a,i}$, i=1,2,..,15) and the average bias count ($B_{a,i}$, i=1,2,..,15) are given by

$$D_{a,i} = \frac{\sum_{r=1}^{200} \sum_{c=1}^{700} D_i[r,c])}{700 \times 200}$$

$$B_{a,i} = \frac{\sum_{r=1}^{200} \sum_{c=1}^{700} B_i[r,c])}{700 \times 200}$$

where r is the specific row and c is the specific column in the sub-frame. The normal dark count (D_0) respectively normal bias count (B_0) is given by

$$D_0 = \frac{\sum_{i=1}^{5} D_{a,i}}{5}$$

$$B_0 = \frac{\sum_{i=1}^{5} B_{a,i}}{5}$$

The normal count is necessary to measure the average excess count per pixel above normal as a function of time after the flat field exposure. The excess dark count ($D_{e,i}$, i=6,7,..,15) and excess bias count ($B_{e,i}$, i=6,7,..,15) are given by

$$D_{e,i} = D_{a,i} - D_0$$

$$B_{e,i} = B_{a,i} - B_0$$

The above experiment was repeated five times. This was done for a number of different temperatures (-10°, -5°, 0°, 5°, 10°, 15°, and 18° Celsius). Each experiment covers 31 frames (15 dark, 15 bias, and 1 flat field frame), i.e. 1085 frames total. To store this data, roughly 300 MBytes are necessary.

4.4 Experimental results I

The results for -10°, 0°, and 10° C are shown in figure 6. The lines in this figure are simply guides for the eye.

One notes immediately that the excess dark count (the "ghost") decays exponentially with time, with the time constant being a strong function of

temperature. Thus one suspects a thermally activated source for these excess dark count electrons.
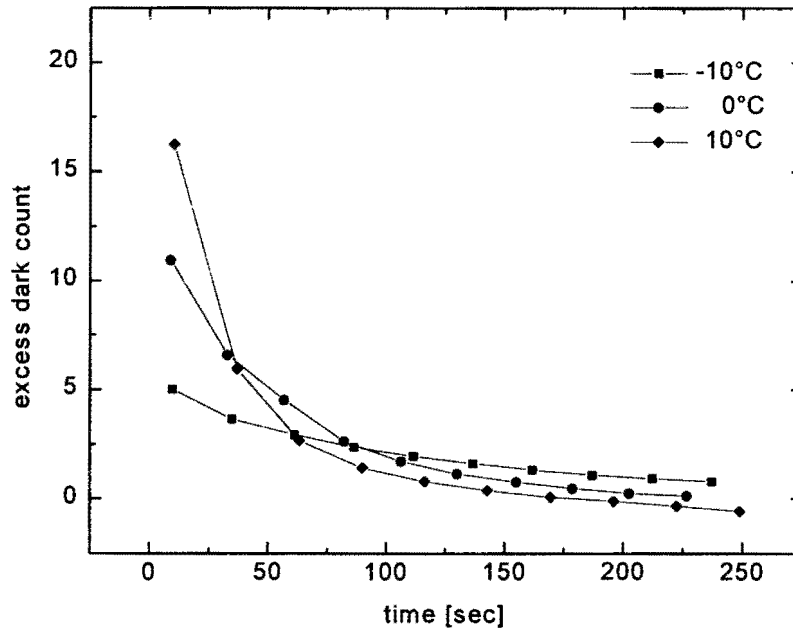
Fig. 6 Excess dark count for a sequence of dark images taken after flat field exposure for several temperatures.

4.5 Model

This study now presents a model, with supporting data, which explains this phenomenon in terms of electrons photo-excited during normal exposures into mid-gap impurity or interface trapping states. These electrons trapped at impurity/interface sites are then thermally excited into the conduction band, are

collected in the pixel potential wells, and appear subsequently as signal or, as in our case, as excess dark count. This is illustrated schematically in figure 7.
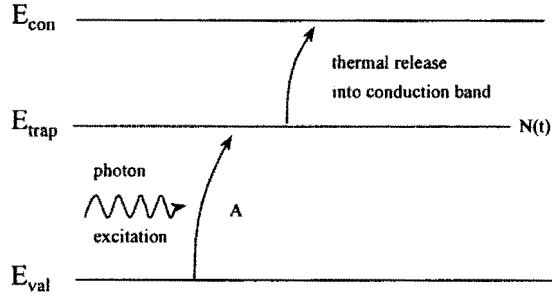
Fig. 7 Schematic diagram of photo-excited electrons moving into and out of trapping sites where $N(t)$ is the number of trapped electrons above thermal equilibrium and A is the photo-conversion efficiency for loading the traps.

Now, the relation between the measured, integrated excess dark count I(t) (as shown in figure 6) and the thermally generated time release of these electrons trapped at impurity/interface sites is examined in detail. In simple terms,

$$I(t) = \int \left| \frac{dN}{dt} \right| dt$$

where dN/dt is the rate of thermal excitation into the conduction band and is proportional to the number of excess occupied trapping sites, N, above the thermal equilibrium value (that is, the excess remaining from optical loading).

The excess population of impurity electrons, N, can be also measured as they decay back to their thermal equilibrium value.

It is expected that the rate of thermal depopulation, dN/dT is proportional to N, so it can be written

$$\frac{dN}{dt} = -rN = -\frac{N}{\tau}$$

which implies

$$N = N_0 \exp\left(-\frac{t}{\tau}\right), \text{ and } \frac{dN}{dt} = -\frac{N_0}{\tau}\exp\left(-\frac{t}{\tau}\right)$$

where τ is the characteristic lifetime of the trapping state. This lifetime should depend on temperature as

$$\tau = \tau_0 \exp\left(\frac{\Delta E}{kT}\right)$$

where (ΔE) is the activation energy of the trapping site – that is, the energy of the trap below the conduction band. A detailed analysis of the excess dark count intensity $I(t)$ should thus give information on both the number (N_0) and characteristic lifetime (or energy) of the traps.

Returning back to the general expression for integrated excess dark count as a function of time, it can be noted that the measured excess dark count, for a given dark exposure at time t_d after the flat field, will include contributions from the trapping sites depopulating (dN/dt) during the preceding flushing time (t_f), the entire dark-exposure time (t_e), and part of the readout time(t_r). The trapping sites will also contribute to the bias count by depopulating during the readout (equivalent to a zero-second dark exposure) and the preceding flush. This is depicted below.
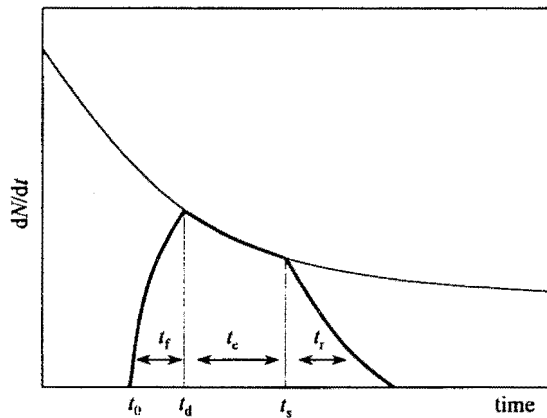
Fig. 8   Illustration showing the collection of excess dark counts due to flushing, dark exposure, and read-out processes.

The measured excess dark count $I(t_d)$ is given by the area under the bold line. The contributions during each time segment, t_f, t_e, and t_r, are explained in detail below.

4.5.1 Flushing

The electrons accumulating in each pixel are constantly being read out (flushed) to avoid the accumulation of thermal dark counts during the downtime between image exposures. These sequential readouts of pixel rows take a time t_f and are interrupted when an exposure is taken (in our case at time t_d). Individual pixel rows then, have been accumulating excess dark count for times ranging from 0 to t_f since they were last read out before the dark exposure (spanning the time t_0 to t_d in the figure above), and so must be included in the integral for $I(t)$. The fraction of pixels receiving thermally-relaxing electrons from trapping sites at time t before the dark exposure, is given by $(t - t_0)/t_f$, and so the integrated contribution to the intensity from the flushing time becomes

$$N_f = \int_{t_0}^{t_0+t_f} \frac{t-t_0}{t_f}\left[\frac{dN}{dt}\right]dt = \int_{t_0}^{t_0+t_f} \left(\frac{-t_0}{t_f}+\frac{t}{t_f}\right)\left(\frac{N_0}{\tau}e^{-t/\tau}\right)dt$$

Integrating by parts and simplifying leads to

$$N_f = \frac{N_0}{t_f}\left[e^{-t_0/\tau}\left(\tau-\left(t_f+\tau\right)e^{-t_f/\tau}\right)\right]$$

which is the expression for the trapping site electrons released during the preceding flush and appearing as excess dark count in the subsequent dark frame.

4.5.2 Dark Exposure

All pixel rows are accumulating thermal counts during the entire dark exposure, and so no weighting factor is needed. The integrated contribution to the excess dark count is given simply by

$$N_d = N_0 \exp\left(-\frac{t_d}{\tau}\right)\left(1 - \exp\left(-\frac{t_e}{\tau}\right)\right)$$

or

$$N_d = N_0 \exp\left(-\frac{t_d}{\tau}\right)\left(1 - \exp\left(-\frac{t_e}{\tau}\right)\right)$$

which represents the excess dark count released by trapping sites during the dark exposure.

4.5.3 Read out

Similar to the case of flushing, the readout takes a finite time t_r and thus the different pixel rows collect dark signal for a time ranging from 0 to t_r after the dark exposure. The integrated contribution from the readout time is given by

$$N_r = \int_{t_x}^{t_x+t_r} \left(1 - \frac{t-t_0}{t_r}\right)\left(-\frac{dN}{dt}\right)dt$$

or

$$N_r = \frac{N_0}{t_r}\left[e^{-t_x/\tau}(-\tau + t_r + \tau e^{-t_r/\tau})\right]$$

Finally, the total excess dark count, $I(t)$, generated by electrons released from trapping sites and collected in a dark exposure taken at time t after the flat field (which loaded the trapping sites) is given by

$$I(t) = N_f + N_d + N_r$$

or

$$I(t) = \frac{N_0}{t_f}\left[e^{-t_0/\tau}(\tau - (t_f + \tau)e^{-t_f/\tau})\right] + N_0 e^{-t_d/\tau}(1 - e^{-t_e/\tau}) + \frac{N_0}{t_r}\left[e^{-t_x/\tau}(-\tau + t_r + \tau e^{-t_r/\tau})\right]$$

This expression has only two independent parameters, N_0, the number of excess electrons loaded into the traps during the flat-field exposure, and τ, the characteristic lifetime of the trapping state which depends on temperature and from which the energy level of the state can be derived.

4.6   Experimental results II

To obtain values for N_0 and τ, the measured excess dark count intensities were fitted against the above expression for $I(t)$. Doing this at different temperatures, T, also determines $\tau(T)$, which is fitted to the expression and from it is obtained a characteristic energy E_t for the trapping states.

A typical fit for $I(t)$ to the data is given in figure 9 where the fit to the raw data for the three temperatures -10°, 0°, and 10° C is showed. As one can see, the agreement between the model and experimental data is quite good.
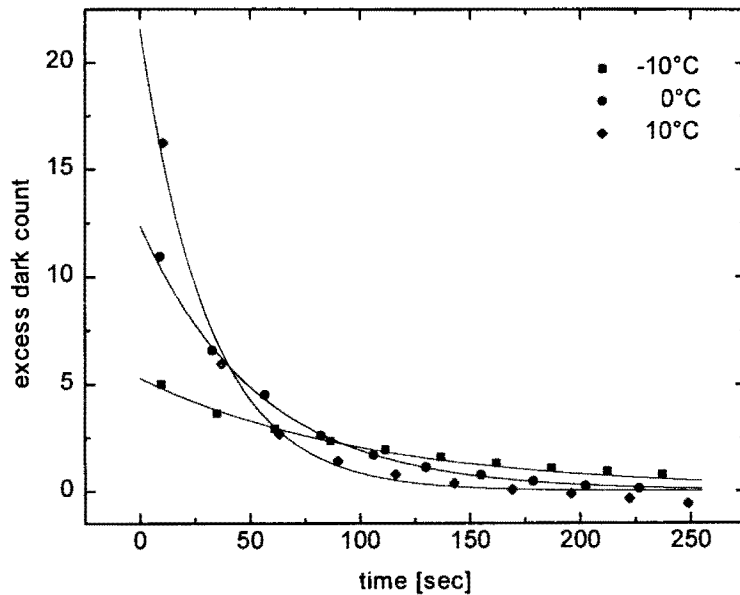
Fig. 9   Excess dark count for a sequence of dark images taken after flat field exposure for several temperatures, including the fitted lines.

From this analysis, values of N_0 which depend on the exposure conditions, can be obtained – that is, the initial number of loaded traps depends on the illumination conditions under which we are optically loading them. This will be discussed in the following section. As mentioned, from the characteristic lifetime for the traps as a function of temperature a trapping energy can be derived. This is shown in figure 10. An energy of 0.48 eV is derived which puts it in the middle of the silicon energy gap.
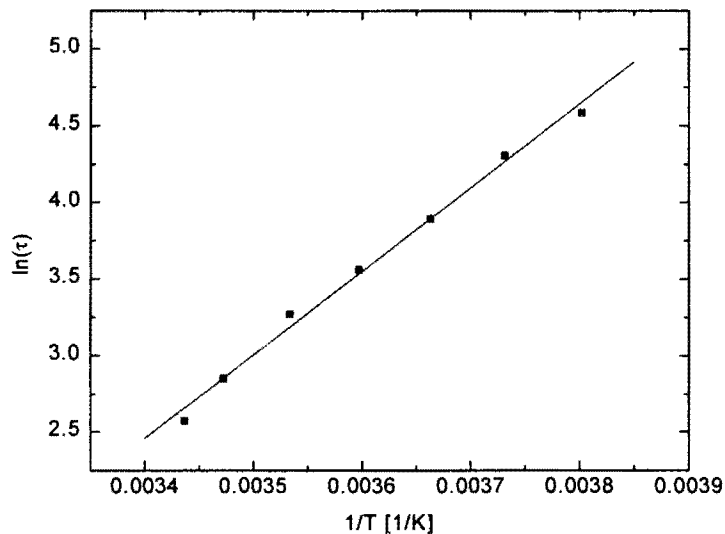
Fig. 10 The logarithm of the characteristic time vs. the inverse of temperature. The slope of the graph yields a characteristic energy level of 0.48 eV.

4.7   The optical loading of trapping states

From the analysis above, N_0, the number of excess traps loaded by optical excitation during the exposure can also be derived. The experiment and analysis were repeated for different flat field exposure times (3, 5, 8, 10, 12, 15, 20, 25, 30, 40, 60, 80, 110, 150, and 200 seconds), different light-intensity conditions (168, 324, and 1140 counts/second) and different temperatures (0°, 5°, and 10° Celsius). Instead of using all possible combinations of light-intensity conditions and temperatures, only six were used for all exposure times. These six combinations are marked in table 1.

	0°C	5°C	10°C
168 counts/sec	✓	✓	✓
324 counts/sec		✓	✓
1140 counts/sec			✓

Tab. 1 The six combinations of light-intensity and temperatures for which N_0 as a function of exposure time was determined.

In order to increase the speed of processing each experiment was repeated only three times. 8370 frames were taken. To store this data, roughly 2.2 GByte were necessary.

4.8   Experimental results III

An interesting effect is seen as shown in figures 11 and 12. Figure 11 shows graphs of N_0 (as derived from the previous analysis) as a function of

exposure times for three different light-intensity conditions. Whereas figure 12 shows graphs of N_0 (as derived from the previous analysis) as a function of exposure times for three different temperatures.
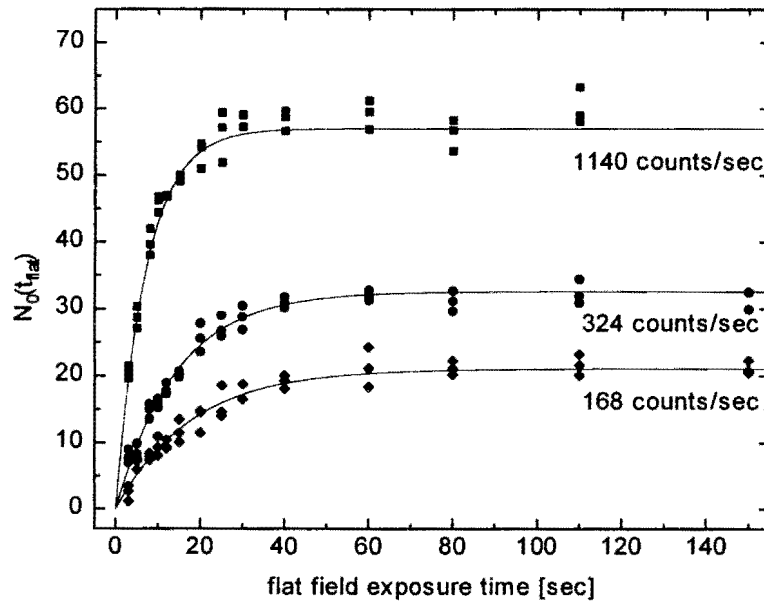
Fig. 11 The number of excess traps loaded as a function of exposure time for three different light-intensity conditions at 10° Celsius.

One notes immediately N_0 saturates after some exposure time and that this saturation depends on the light intensity and temperature. This is understood, and the fits explained, by considering the following:

Figure 7 depicts the optical loading of the trapping sites above their thermal equilibrium values. During exposure, the traps are loaded (above their

thermal equilibrium value) by optical pumping and are subsequently thermally excited into the conduction band. The time rate of change of excess loaded traps is then given by

$$\frac{dN}{dt} = A(N) - \frac{N}{\tau}$$

where $A(N)$ represents the rate of optical excitation from the valence band into the trapping sites. It depends on the number of available (unoccupied) trapping sites

$$A(N) = \left(1 - \frac{N}{N_{\text{max}}}\right)A_0$$

where A_0 is an optical excitation rate or cross section, N_{max} is the number of trapping sites, and $(1 - N/N_{\text{max}})$ is the fraction of available trapping sites. This leads to

$$\frac{dN}{dt} = A_0 - \frac{N}{N_{\text{max}}}A_0 - \frac{N}{\tau} = A_0 - \left(\frac{A_0}{N_{\text{max}}} + \frac{1}{\tau}\right)N \equiv A - \frac{N}{\tau'}$$

with

$$\tau^{'} = \left(\frac{A_0}{N_{max}} + \frac{1}{\tau} \right)^{-1}$$

Therefore now an expression for N_0 (the initial number of loaded traps at time 0) can be obtained:

$$\int_0^{N_0} \frac{dN}{A - \frac{N}{\tau'}} = \int_0^t dt$$

which leads to

$$N_0 = A_0 \tau' \left(1 - e^{-\frac{t}{\tau'}} \right)$$

The expression for N_0 contains two independent parameters, A_0 (the cross-section for optical excitation into a trapping site) and N_{max}, the maximum available trapping sites per pixel.

This expression was applied to the data and the fits in figures 11 and 12 obtained from a *single* fitting of all the data; fitting a single N_{max} and A_0 for all the data. The fit matches the data very well (as seen in figures 11 and 12), and yields values of A_0=0.007 and N_{max}=80.98.
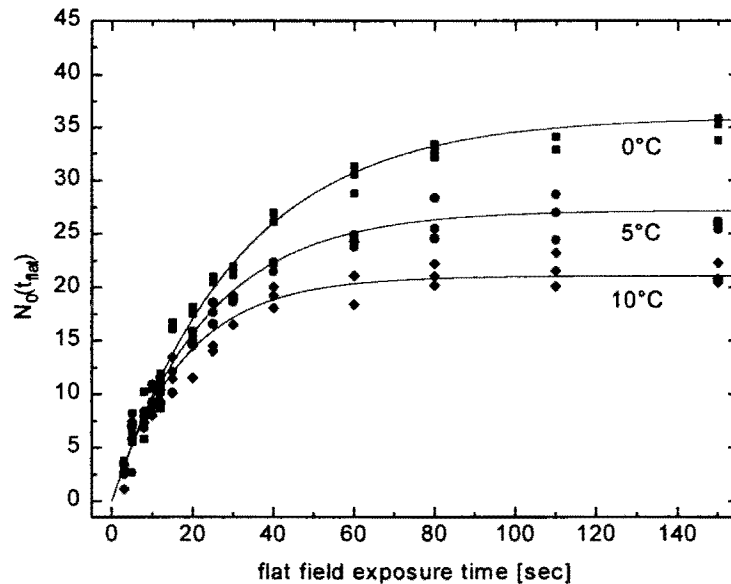
Fig. 12   The number of excess traps loaded as a function of exposure time for three diffrent temperatures for a light-intensity condition of 167 counts/sec.

4.9   Conclusions

In this study the phenomena of residual bulk, or ghost, images in CCD imagers has been systematically analyzed. An explanatory model and statistical analysis technique have been developed which enables the derivation of the densities and the characteristic energies for the impurity states responsible for these effects. These residual images are a source of unwanted signal (i.e., noise) in subsequent frames, and should be considered whenever very exact, low light-level signal processing is necessary. The techniques/analysis can also be used

by manufacturers to gain important information regarding the nature and densities of impurity states in CCD chips.

5 Systematic study of dark current

5.1 Introduction

Dark current noise from the pixels of an image sensor limits the dynamic range of the sensor and may, in the case of an individually noisy pixel, cause "white spot" or "hot pixel" defects that affect device yield. Dark current is illustrated in figure 13 showing a dark frame taken with an exposure time of 500 sec at a temperature of 18° Celsius. It can be observed that pixels with a higher dark current are randomly distributed in the CCD imager. The dark count range in this case is between a few and a couple of thousand counts.

Fig. 13 Dark frame taken with an exposure time of 500 seconds at 18° Celsius (Kodak CCD imager KAF 1600-2).

For most of the pixels (>90%) of the CCD imager the dark current at 18° Celsius is roughly 1.5 counts/seconds. With a count limit of 32,000 counts due to the computer interface the CCD detector could be dark exposed for almost 6 hours. However some of the "hot pixels" have a dark current of 50 counts/second or more. Therefore the count limit is already reached after 8 minutes. This limitation is shown in figures 14 and 15. Figure 14 illustrates a dark count histogram for 10 seconds dark exposure and figure 15 for 500 seconds dark exposure. In both cases the CCD imager was exposed at 18° Celsius.
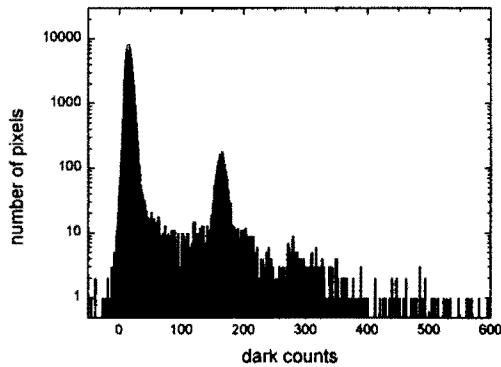
Fig. 14 Dark count histogram for 10 seconds dark exposure at 18° Celsius.
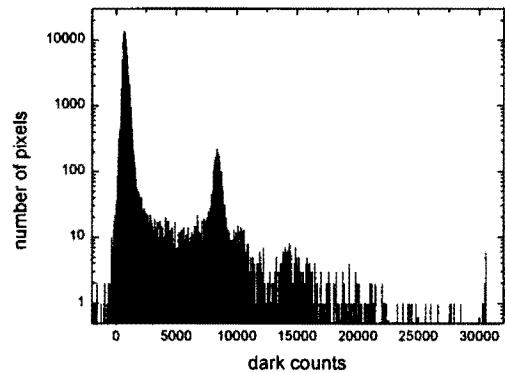
Fig. 15 Dark count histogram for 500 seconds dark exposure at 18° Celsius.

Dark current is generally linear in time. This can be observed in figure 15. The dark count increases with a higher dark exposure time. In addition

figure 15 shows that single pixels reach the count limit within 500 seconds dark exposure.

This thesis covers a detailed study of dark current and hot pixels. Furthermore, an analysis technique is described that enables the derivation of characteristic energies responsible for these effects.

5.2 Experimental

To understand the nature of dark current, a systematic study of their time and temperature dependence is performed. The examined imager was the Kodak KAF 1600-2 sensor. In order to increase the speed of processing and to save memory a 392x258 pixel sub-frame was used. For different temperatures (-10°, -5°, 0°, 5°, 10°, 15°, and 18° Celsius) and different dark exposure times (3, 5, 10, 20, 35, 50, 100, 200, 300, 400, and 500 seconds) dark and bias frames were alternately taken. For each temperature 15 dark and bias frames were conducted for short exposure times (3, 5, 10, 20, and 35 seconds) and 5 dark and bias frames were conducted for longer exposure times (50, 100, 200, 300, 400, and 500 seconds). Each temperature covered 105 frames, i.e. 735 frames total. To store this data, roughly 500 MBytes were necessary.

Now, one must consider that the raw dark count (D) obtained in the readout of each pixel after a dark exposure contains the raw bias count (B). Therefore the raw bias count has to be subtracted from the raw dark count to

determine the "pure" or calibrated dark count (C). The calibrated dark count for each pixel is given by

$$C(r,c) = D(r,c) - B(r,c) \qquad r = 1,2,..,258,\ c = 1,2,..,392$$

where r is the specific row and c is the specific column of the CCD imager.

From the calibrated dark count data (C) the "medium" average dark count (M) was calculated for each pixel at each temperature and each dark exposure time. To calculate the medium average all data points except the lowest and highest data points were used. For short exposure times (3, 5, 10, 20, and 35 seconds) the three highest and three lowest data points were not used; and for long dark exposure times (50, 100, 200, 300, 400, and 500 seconds) the highest and lowest data point were not used. This technique reduces the influence of cosmic ray events in single pixels with random positions.[16] Therefore only 9 data points were used for short exposure times and 3 data points for long exposure times to calculate the average dark count for each pixel at each temperature and each exposure time. The equation is given by

$$M(T,t,r,c) = \frac{\sum_{i=1}^{n} C(T,t,r,c)}{n}$$

where T is the temperature, t is the dark exposure time, r is the specific row, and c is the specific column of the CCD imager.

5.3   Distribution

Pixels with lower or higher dark current are randomly distributed in the CCD imager, but the dark current for pixels is not equally distributed across the CCD detector. Figures 16 and 17 show dark current histograms for different dark exposure times at 18° Celsius. Figure 16 shows the dark current histogram where the dark current was calculated for each pixel from a dark frame exposed for 5 seconds to a dark frame exposed for 10 seconds. Figure 17 shows the current histogram where the dark current was calculated for each pixel from a dark frame exposed for 400 seconds to a dark frame exposed for 500 seconds.
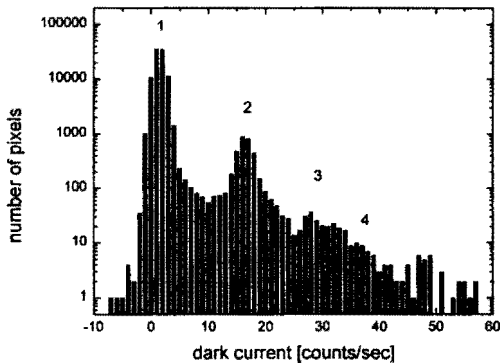
Fig. 16   Dark current histogram calculated from dark frame exposed for 5 seconds to dark frame exposed for 10 seconds at 18° Celsius.
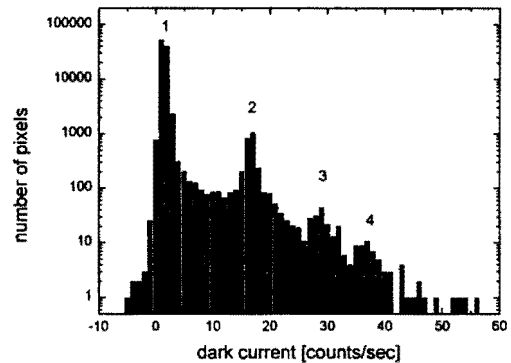
Fig. 17   Dark current histogram calculated from dark frame exposed for 400 seconds to dark frame exposed for 500 seconds at 18° Celsius.

A quantization of dark current can be observed in the histograms. This has been reported previously by McGraph et al.[17] in 1987. Two different deep-level traps were found to be responsible, but their identities were unknown. In 1992 a "dark current spectroscopy" was developed by McColgin et al.[18] to identify and monitor specific deep-level traps that may occur in imagers. They reveal four different deep-level traps that produce characteristic quantization in the imager dark current. Three of these traps were found to exist in gold, cobalt, and nickel.

Comparing figures 16 and 17, it can be observed that the peaks (*1, 2, 3,* and *4*) are localized in the same positions. Pixels in these regions are mainly pixels with a linear dark count behavior in time. However, it can be seen that not as many single pixels with a high dark current (>40 counts/second at 18° Celsius) for short exposure times occur in figure 17 as in figure 16. These are pixels with a non-linear dark count behavior in time.

5.4 Classification

The pixels of the CCD imager were classified and split into several groups based on their dark count behavior in time. The first group are "negative pixels". These pixels have a negative dark current which is not consistently linear over the dark exposure time. This group includes roughly three percent of all pixels and is randomly distributed across the CCD imager. The remaining pixels were split into a group of "linear pixels" with a dark count behavior

linear in time and a group of "non-linear pixels" with a dark count behavior non-linear in time. Finally the "linear pixels" were split into five sub groups: "normal pixels", "hot pixels", "hot peak 3", and "hot peak 4", and "remaining pixels". The classification is shown in figure 18.
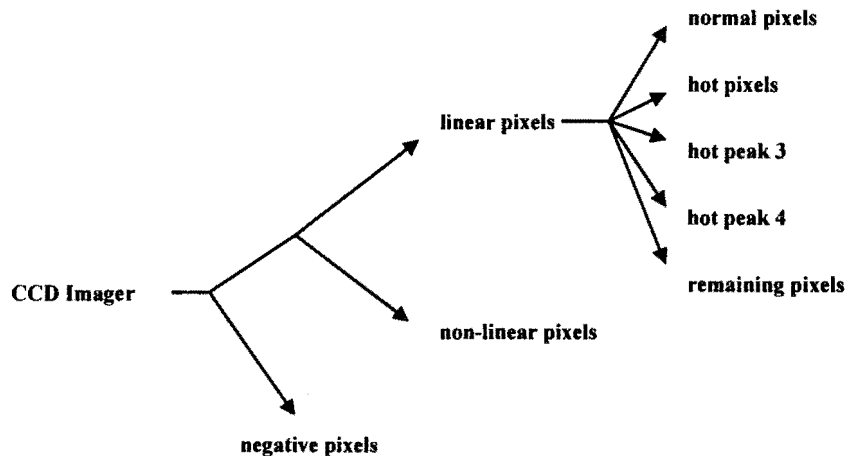
Fig. 18 The pixels of the CCD imager are classified and split into a group of "negative pixels" (5%), a group of "non-linear pixels" (2.5%), and in four groups of "linear pixels" ("normal pixels" (89%), "hot pixels" (2.5%), "hot peak 3" (0.2%), "hot peak4" (0.1%), and "remaining pixels") (the percentage represents the number of pixels in each group).

The "normal pixels" include pixels with a linear dark count behavior over time and a dark current between 0 and 4 counts/second at 18° Celsius. Thus these pixels correspond to the first peak in figure 17. This group includes roughly 90 percent of all pixels and is randomly distributed across the CCD imager. The group of "hot pixels" includes pixels with a linear dark count behavior over time and a dark current between 15 and 18 counts/second at 18°

Celsius. Thus these pixels correspond to the second peak in figure 17. This group includes roughly 2.5 percent of all pixels and is randomly distributed across the CCD imager. The group of "hot peak 3" includes pixels with a linear dark count behavior over time and a dark current between 27 and 30 counts/second at 18° Celsius. Thus these pixels correspond to the third peak in figure 17. This group includes roughly 0.2% of all pixels and is randomly distributed across the CCD imager. And finally, the group of "hot peak 4" includes pixels with a linear dark count behavior over time and a dark current between 36 and 39 counts/second at 18° Celsius. Thus these pixels correspond to the fourth peak in figure 17. This group includes roughly 0.1% of all pixels and is randomly distributed in the CCD imager. The pixels in the "hot peak 3" and "hot peak 4" groups were not investigated further in the research for this thesis. The histograms of the dark current for each group is shown in figure 19.
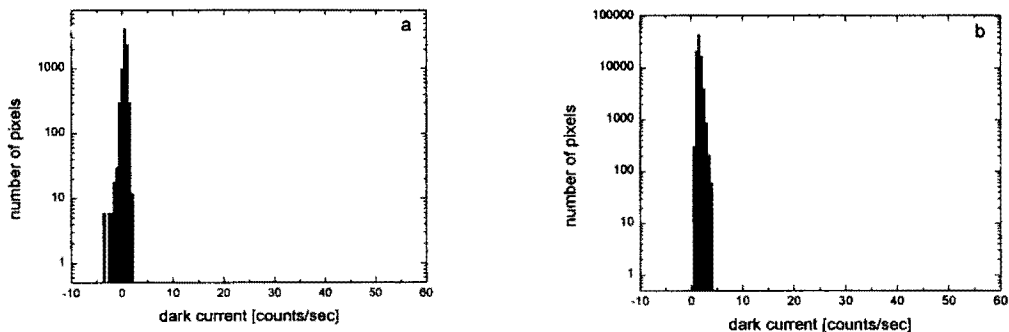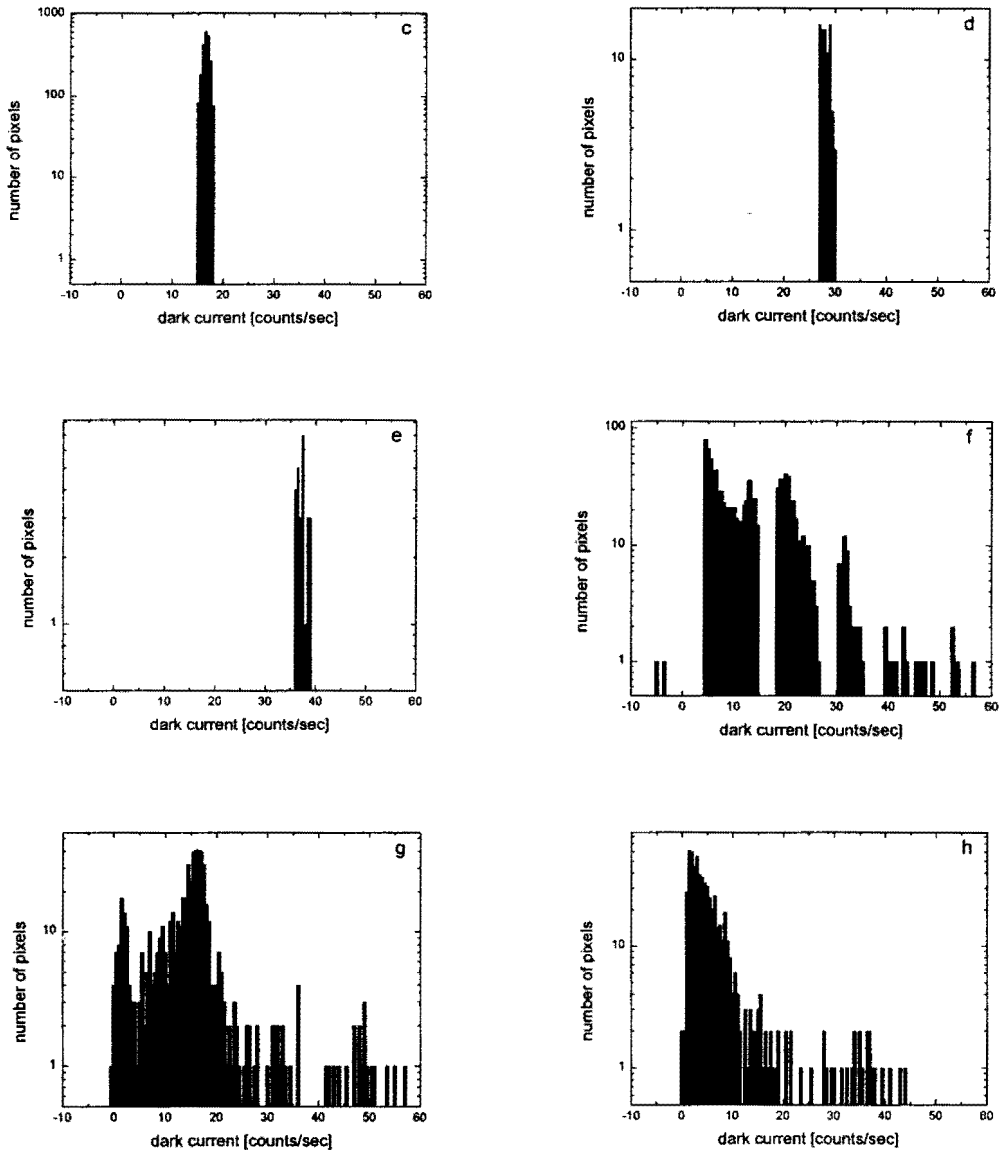
Fig. 19   Dark current histograms for the different pixel groups (a = negative pixels, b = normal pixels, c = hot pixels, d = hot peak 3, e = hot peak 4, f = remaining pixels, g and h = non-linear pixels). All figures show dark current histograms calculated from dark frames exposed for 400 seconds to dark frames exposed for 500 seconds at 18° Celsius, except figure g, which shows a dark current histogram calculated from dark frames exposed for 5 seconds to dark frames exposed for 10 seconds at 18° Celsius.

5.5 Negative pixels

Figures 20 and 21 show examples of pixels from the group of negative pixels. The dark current is neither always negative, linear in time nor negative for all temperatures. Figure 21 shows an example where the dark current becomes positive for higher temperatures.

Fig. 20 Dark count as a function of exposure time for different temperatures for an example negative pixel. The position in the CCD imager is row=107 and column=347. In this case the dark current is negative for all temperatures.

Fig. 21 Dark count as a function of exposure time for different temperatures for an example negative pixel. The position in the CCD imager is row=109 and column=288. In this case the dark current becomes positive for 15° and 18° Celsius.

5.6 Linear pixels

The group of linear pixels was split into five sub groups. The following figures show examples of normal pixels and hot pixels.

5.6.1   Normal pixels

Figure 22 shows the dark count as a function of exposure time for different temperatures for a normal pixel. Whereas figure 23 shows the dark current as a function of inverse temperatures corresponding to the pixel shown on the left side.

Fig. 22   Dark count as a function of exposure time for different temperatures for an example normal pixel. The position in the CCD imager is row=100 and column=231. There were 89% pixels in the CCD imager with similar results.

Fig. 23   Dark current as a function of inverse temperatures for an example normal pixel shown in figure 22.

5.6.2   Hot pixels

Figure 24 shows the dark count as a function of exposure time for different temperatures for a hot pixel. Whereas figure 25 shows the dark current as a function of inverse temperatures corresponding to the pixel shown on the left side.
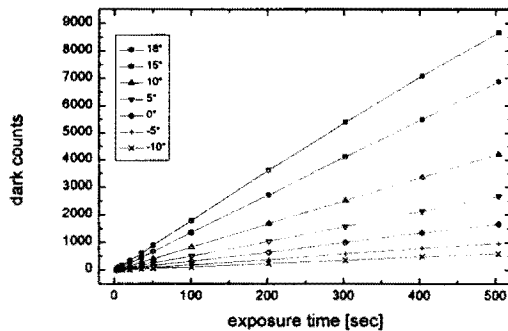
Fig. 24 Dark count as a function of exposure time for different temperatures for an example hot pixel. The position in the CCD imager is row=100 and column=275. There were 2.5% pixels in the CCD imager with similar results.
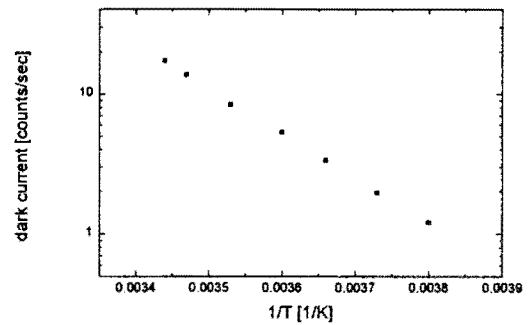
Fig. 25 Dark current as a function of inverse temperature for an example hot pixel shown in figure 24.

5.7 Non-linear pixels

Non-linear pixels have a higher dark current for short exposure times and a lower dark current for longer exposure times. The dark current for short exposure times is at least twice as high as for normal pixels, whereas the dark current for longer exposure times moves towards the dark current of normal pixels (this can be seen in figure 19h). Figures 26 and 27 show the dark count as a function of exposure time for different temperatures for two non-linear pixels.

It can be observed that the dark current is higher for shorter exposure times. For some non-linear pixels the dark current for shorter exposure times is even higher than 50 counts/second and was therefore seen in figure 17.
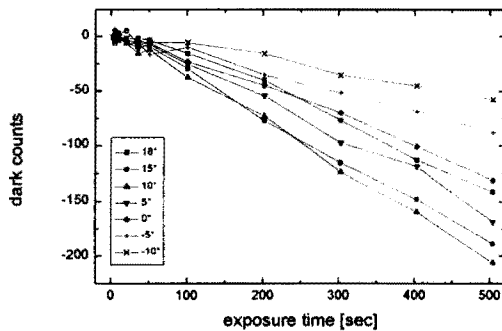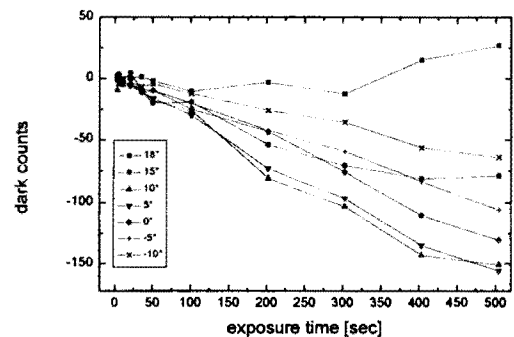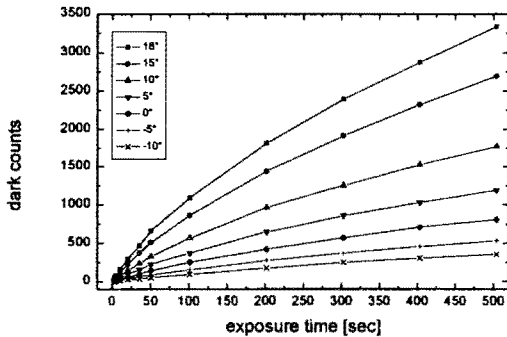
Fig. 26 Dark count as a function of exposure time for different temperatures for an example non-linear pixel. The position in the CCD imager is row=100 and column=166.

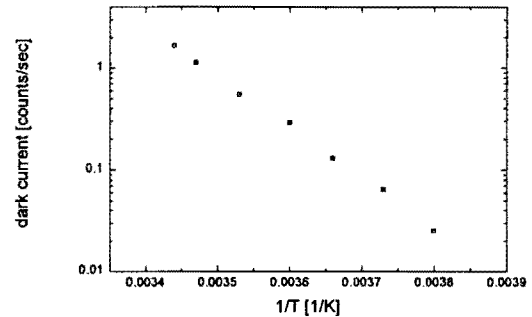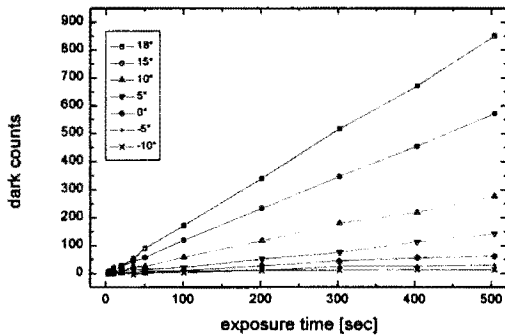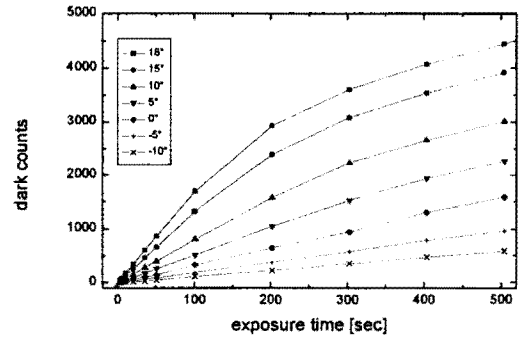**Fig. 27** Dark count as a function of exposure time for different temperatures for an example non-linear pixel. The position in the CCD imager is row=100 and column=278.

5.8 Nearest neighbors

Pixels from all groups are randomly distributed in the CCD imager. There is no specific pattern and no specific area in which one kind of pixel mainly exists. But there is a correlation between negative pixels and hot pixels, hot peak3, hot peak4, and non-linear pixels. The right neighbor of a pixel from the group of hot pixels, hot peak 3, hot peak 4 or non-linear pixels is always either a pixel from one of the groups listed above or a negative pixel. This can be observed in figure 29. Figure 28 shows the distribution of negative pixels in the CCD imager and figure 29 shows the distribution of negative pixels without a left neighbor from the group of hot pixels, hot peak 3, hot peak 4, remaining pixels, and non-linear pixels.

Fig. 28 Distribution of negative pixels in the CCD imager.

Fig. 29 Distribution of negative pixels which do not have a left neighbor from the following groups: hot pixels, hot peak 3, hot peak 4, remaining pixels, and non-linear pixels.

Comparing figures 28 and 29, it can be observed that the majority of negative pixels are not isolated in the CCD imager. They are rather the right neighbor to pixels from the group of hot pixels, hot peak 3, hot peak 4, remaining pixels, and non-linear pixels.

This result becomes more clear by investigating the dark current of the left neighbor pixels of negative pixels. Figures 30 and 31 show the dark current histogram of left neighbor pixels of negative pixels at different dark exposure times at 18° Celsius.

Comparing figures 17 and 31, the correlation between negative pixels and hot pixels, hot peak 3, hot peak 4, and non-linear pixels can be observed. The peaks in figures 17 and 31 are at the same position and the number of pixels in each peak are almost the same.
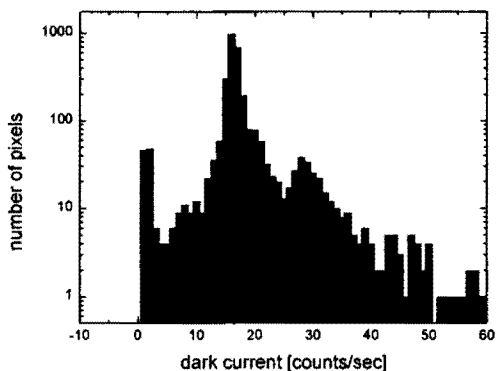
Fig. 30 Dark current histogram of left neighbors of negative pixels calculated from dark frame exposed for 10 seconds to dark frame exposed for 20 seconds at 18° Celsius.
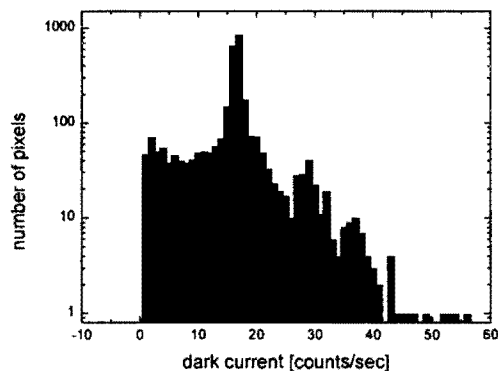
Fig. 31 Dark current histogram of left neighbors of negative pixels calculated from dark frame exposed for 400 seconds to dark frame exposed for 500 seconds at 18° Celsius.

The existence of negative pixels is probably caused in the charge detection amplifier when a small charge packet is read out after a big charge packet. This would explain, why negative pixels only appear as a right neighbor.

5.9 Model

One notes immediately that the dark count is generally linear in time, with the dark current being a strong function of temperature. Thus a thermally activated source for these dark count electrons is expected. The following presents a model for each pixel group, with supporting data. This explains the dark counts in terms of electrons which are thermally released from the valence band to the conduction band or electrons which thermally "hop" from the valence band into interface states and then to the conduction band.

For each pixel group an analytic technique is described to examine in detail the relation between the measured dark count $I(t)$ and the thermally generated electrons within the device. In simple terms,

$$I(t) = \left| \frac{dN}{dt} \right| t$$

where dN/dt is the rate of thermal release into the conduction band and t is the dark exposure time.

5.9.1 Linear pixels

Figure 32 shows the model for normal pixels. For normal pixels it is assumed that the dark current is due to thermally generated electrons and diffusion in the neutral bulk or depletion region.

E_C

thermal release into conduction band

E_I

$\frac{dN_v}{dt}$

E_V

Fig. 32 Model for normal pixels.

Thus it can be expected that the dark current rate of thermal release into the conduction band, dN_v/dt is proportional to N_v, the number of free carriers. This can be written as

$$\frac{dN}{dt} \equiv \frac{dN_v}{dt} = -\frac{N_v}{\tau_v}$$

where τ_v is the characteristic time constant. The number of free carriers N_v is nearly independent of temperature and does not decrease with thermal release to the conduction band, because the holes left behind move to the substrate. Therefore N_v can be written as a constant N_{v0}. The time constant τ_v depends on temperature and can be written as

$$\tau_v = \tau_{v0} \exp\left(-\frac{\Delta E_v}{kT}\right)$$

where ΔE_v is the activation energy for the electrons, k is the Boltzmann constant, and T is the temperature. Therefore the dark count for normal pixels can be written as

$$I(t) = \frac{N_v}{\tau_v} t = \frac{N_{v0}}{\tau_{v0}} \exp\left(\frac{\Delta E_v}{kT}\right) t$$

A detailed analysis of the dark count should thus give information on both the number N_{v0} and the characteristic time constant (or energy).

Figure 33 shows the model for hot pixels. Hot pixels have a significantly higher dark current.

Fig. 33   Model for hot pixels.

In addition to the electrons thermally released from the valence band to the conduction band it is assumed that electrons thermally "hop" from the valence band into impurity states and then to the conduction band. The dark current rate of thermal release into the conduction band can be written as

$$\frac{dN}{dt} = \frac{dN_c}{dt} + \frac{dN_v}{dt}$$

where dN_c/dt is the dark current rate thermally released from the impurity states to the conduction band and dN_v/dt is the dark current rate thermally released from the valence band to the conduct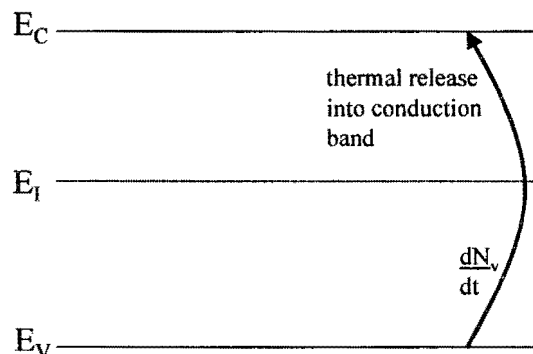ion band. It can be expected that the dark current rate of thermal release into the conduction band, dN_c/dt is proportional to N_i, the number of filled traps in the impurity states. This can be written as

$$\frac{dN_c}{dt} = -\frac{N_i}{\tau_i}$$

where τ_i is the characteristic time constant. The number of traps is nearly independent of temperature. For hot pixels it is assumed that the thermal release into the impurity states dN_f/dt keeps the number of filled traps on a constant level. Thus the number of filled traps N_i does not decrease with thermal release into the conduction band. Therefore N_i can be written as a constant N_{i0} and τ_i can be written as

$$\tau_i = \tau_{i0} \exp\left(-\frac{\Delta E_i}{kT}\right)$$

where ΔE_i is the activation energy for the electrons, k is the Boltzmann constant, and T is the temperature. Using the equation for dN_v/dt from above, the dark count for hot pixels can be written as

$$I(t) = \frac{N_i}{\tau_i}t + \frac{N_v}{\tau_v}t = \frac{N_{i0}}{\tau_{i0}}\exp\left(\frac{\Delta E_i}{kT}\right)t + \frac{N_{v0}}{\tau_{v0}}\exp\left(\frac{\Delta E_v}{kT}\right)t$$

A detailed analysis of the dark count should thus give information on both the number N_{i0} and the characteristic time constant (or energy).

5.9.2 Non-linear pixels

A slightly different model had to be developed for the non-linear pixels. These pixels show an exposure time dependence in addition to the temperature dependence. The model is shown in figure 34.
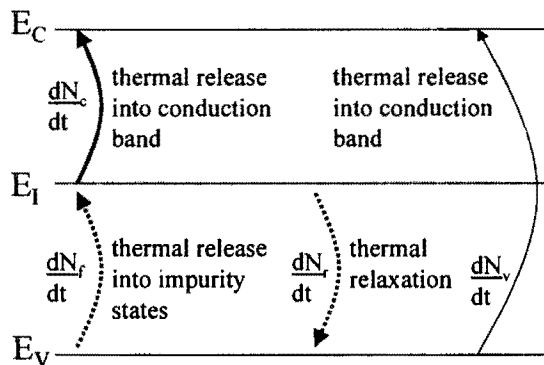
Fig. 34   Model for non-linear pixels.
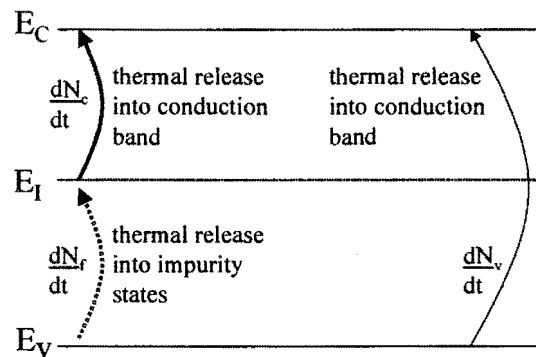
Once again, in addition to the electrons thermally released from the valence band to the conduction band it is assumed that electrons thermally "hop" from the valence band into interface states and then to the conduction

band, but this time the number of filled traps in the impurity states N_i depletes in time. The change in N_i can be written as

$$\frac{dN_i}{dt} = \frac{dN_c}{dt} + \frac{dN_r}{dt}$$

where dN_c/dt is the dark current rate thermally released from the impurity states to the conduction band and dN_r/dt is the rate thermally released from the impurity states. It can be expected that both rates of thermal release are proportional to N_i, the number of filled traps in the impurity states. This can be written as

$$\frac{dN_c}{dt} = -\frac{N_i}{\tau_i}, \text{ and } \frac{dN_r}{dt} = -\frac{N_i}{\tau_r}$$

where τ_i and τ_r are the characteristic time constants for the electrons and can be written as

$$\tau_i = \tau_{i0}\exp\left(-\frac{\Delta E_i}{kT}\right), \text{ and } \tau_r = \tau_{r0}\exp\left(-\frac{\Delta E_r}{kT}\right)$$

where ΔE is the activation energy for the electrons. Thus, dN_i/dt can be written as

$$\frac{dN_i}{dt} = -\frac{N_i}{\tau_i} - \frac{N_i}{\tau_r} = -\frac{N_i}{\tau'}, \quad \frac{1}{\tau'} = \frac{1}{\tau_i} + \frac{1}{\tau_r}$$

which implies

$$N_i = N_{i0} \exp\left(\frac{-t}{\tau'}\right)$$

Combining this result with the dark current rate of thermal release from impurity states into the conduction band, dN_c/dt can be written as

$$\frac{dN_c}{dt} = -\frac{N_i}{\tau_i} = \frac{N_{i0}}{\tau_i} \exp\left(\frac{-t}{\tau'}\right)$$

Thus, using the equation for dN_v/dt from above, the dark count for non-linear pixels can be written as

$$I(t) = \int_0^{t'} \frac{N_{i0}}{\tau_i} \exp\left(\frac{-t}{\tau'}\right) dt + \frac{N_{v0}}{\tau_{v0}} \exp\left(\frac{\Delta E_v}{kT}\right) t$$

$$I(t) = -\frac{N_{i0}}{\tau_i}\tau'\left(1-\exp\left(\frac{-t}{\tau'}\right)\right)+\frac{N_{v0}}{\tau_{v0}}\exp\left(\frac{\Delta E_v}{kT}\right)t$$

$$I(t) = -\frac{N_{i0}}{\tau_{i0}}\exp\left(\frac{\Delta E_i}{kT}\right)\tau'\left(1-\exp\left(\frac{-t}{\tau'}\right)\right)+\frac{N_{v0}}{\tau_{v0}}\exp\left(\frac{\Delta E_v}{kT}\right)t$$

5.10 Experimental results

5.10.1 Linear pixels

Using the equations from above, the normal pixels and the hot pixels have been fitted. A typical fit for normal pixels and hot pixels to the data is shown in figure 35.
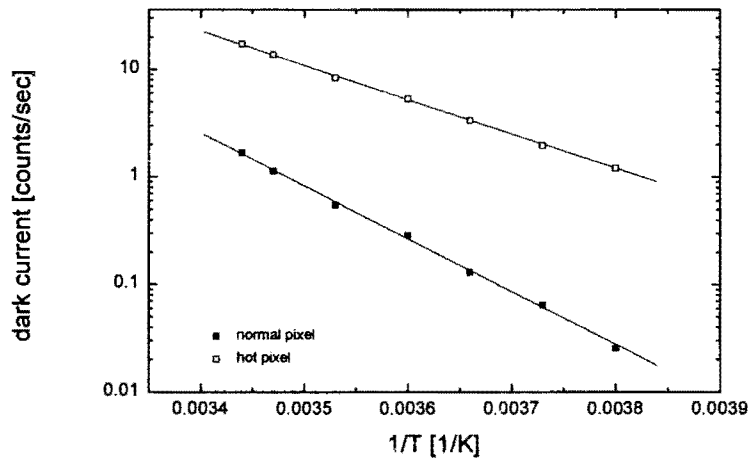

Fig. 35 Dark current as a function of inverse temperature. The lower curve is obtained for the normal pixel shown in figure 22 including the fitted line. The activation energy for this pixel is ΔE=0.98 eV. The upper curve is obtained for the hot pixel shown in figure 24 including the fitted line. The activation energy for this pixel is ΔE=0.63 eV.

Figures 36 and 37 show the results for $ln(N_{v0}/\tau_{v0})$ and ΔE_v for normal pixels.

Fig. 36 Logarithm of the ratio N_{v0}/τ_{v0} as a function of the activation energy for normal pixels.

Fig. 37 Histogram of the activation energy for figure 36. The peak shows an activation energy of 1.05 eV.

The Kodak detector works in MPP mode. In this mode the interface state generation at the $Si\text{-}SiO_2$ is suppressed. The contribution from the bulk should be the main dark source. The measured activation energy is 1.05 eV, in good agreement with an expected activation energy of 1.1 eV.[19]

Figures 38 and 39 show the results for $ln(N_{i0}/\tau_{i0})$ and ΔE_i for hot pixels. The measured activation energy for hot pixels in figure 38 is 0.62 eV. This is in good agreement with the expected activation energy of the interface state generated component of the dark current.

Fig. 38 Logarithm of the ratio N_{i0}/τ_{i0} as a function of the activation energy for hot pixels.

Fig. 39 Histogram of the activation energy for figure 38. The peak shows an activation energy of 0.62 eV.

Figure 40 shows the results for normal pixels and hot pixels.

Fig. 40 Logarithm of the ratio N_{v0}/τ_{v0} or N_{i0}/τ_{i0} as a function of the activation energy. The results for normal pixels and hot pixels are shown.

It can be observed that $ln(N_{v0}/\tau_{v0})$ is proportional to the activation energy ΔE_v for normal pixels and that $ln(N_{i0}/\tau_{i0})$ is proportional to ΔE_i for hot pixels. The proportionality is in good agreement with the compensation law.[20]

5.10.2 Non-linear pixels

The non-linear pixels were analyzed in two different ways. The dark count of pixels from this group is nearly linear in time for very short exposure times (3, 5, and 10 seconds). The dark count points for the exposure times 3, 5, and 10 seconds have been fitted with the linear equations for hot pixels from above. The model for non-linear assumes the same mechanism for thermal release from the impurity states into the conduction band as for hot pixels. Thus similar results are expected. Figures 41 and 42 show the results.
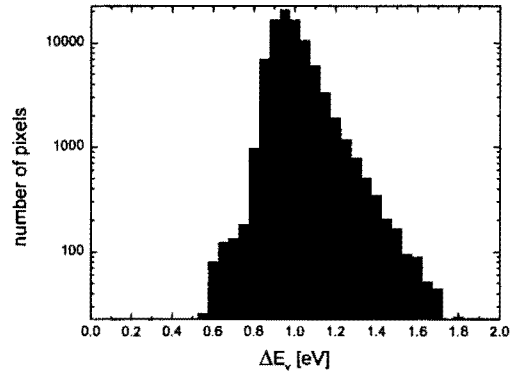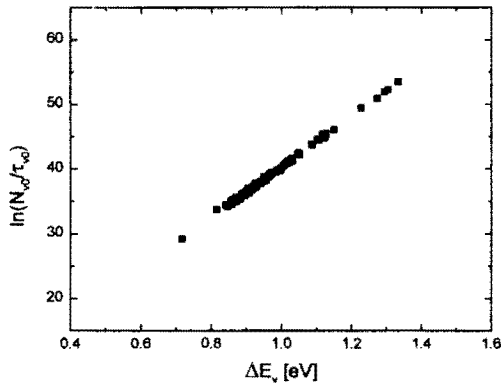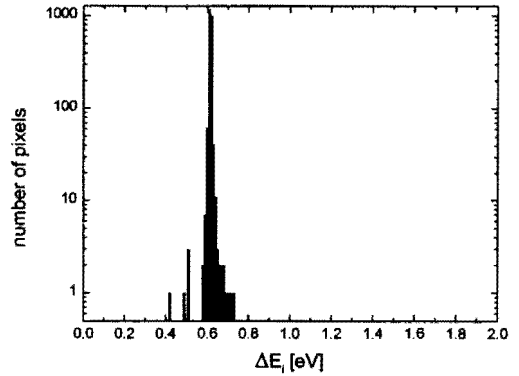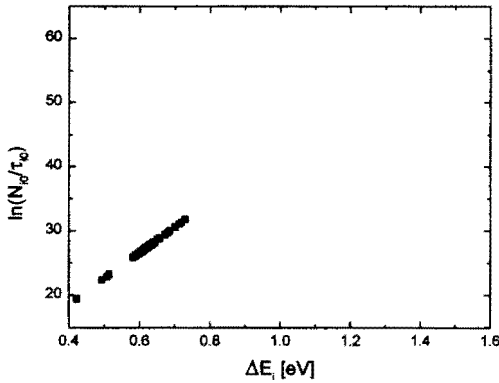

Fig. 41 Logarithm of the ratio N_{i0}/τ_{i0} as a function of the activation energy for non-linear pixels.

Fig. 42 Histogram of the activation energy for figure 41. The peak shows an activation energy of 0.65 eV.

Once again, *ln(N_{i0}/τ_{i0})* is proportional to the activation energy *ΔE_i* and figure 42 shows that the peak for the activation energy is at 0.65 eV. This is in good agreement with the results from hot pixels.

In addition, figure 43 shows the results for normal pixels, hot pixels, and non-linear pixels. It can be observed that for each group *τ* is proportional to the activation energy *ΔE*. Furthermore, the results for hot pixels and non-linear pixels fall on the same line.
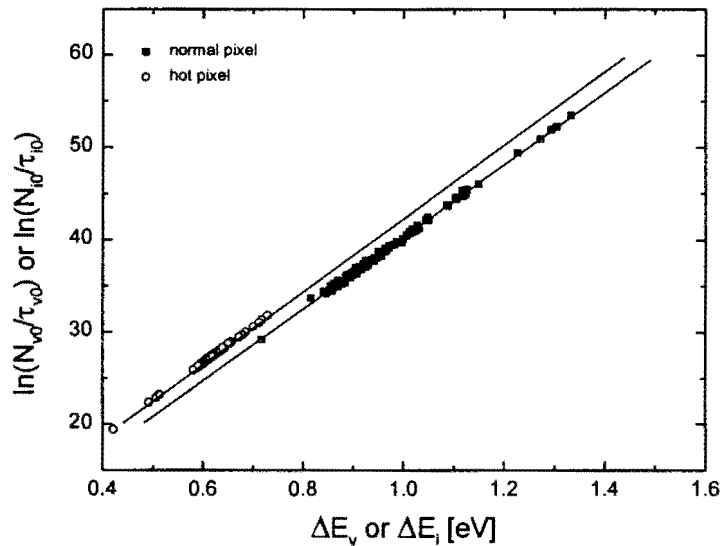

Fig. 43   Logarithm of the ratio *N_{v0}/τ_{v0}* or *N_{i0}/τ_{i0}* as a function of the activation energy. The results for normal pixels, hot pixels, and non-linear pixels are shown.

The second way to analyze was to use the fit equation from the model to calculate N_{v0}/τ_{v0}, ΔE_v, τ'_0, $\Delta E'$, N_{i0}/τ_{i0}, and ΔE_i. Figures 44 and 45 show the results for N_{i0}/τ_{i0} and ΔE_i.
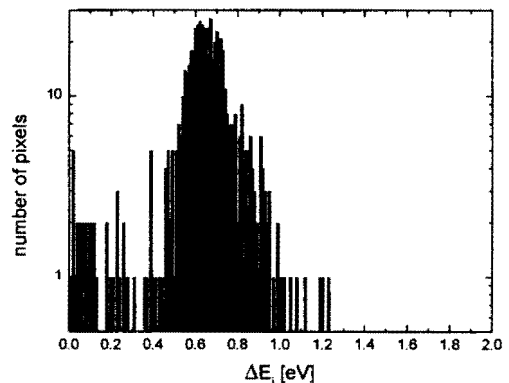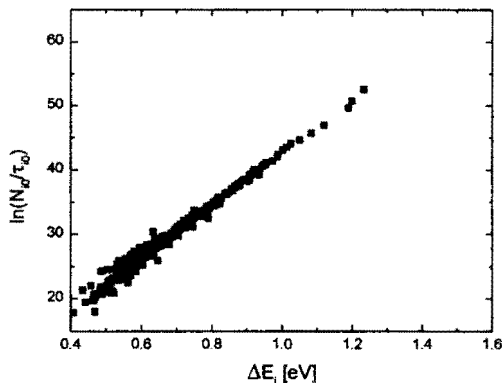

Fig. 44 Logarithm of the ratio N_{i0}/τ_{i0} as a function of the activation energy for non-linear pixels.

Fig. 45 Histogram of the activation energy for figure 44. The peak shows an activation energy of 0.65 eV.

The measured activation energy is 0.65 eV, in good agreement with the expected activation energy shown in figure 42. This data supports the assumption that the thermal release from the impurity states to the conduction band is caused by the same mechanism as shown before in figure 42.

Figure 46 shows the results for normal pixels, hot pixels, and non-linear pixels. It can be observed that $ln(N_{i0}/\tau_{i0})$ respectively $ln(N_{v0}/\tau_{v0})$ is proportional to the activation energy ΔE_{i0} respectively ΔE_{v0}.
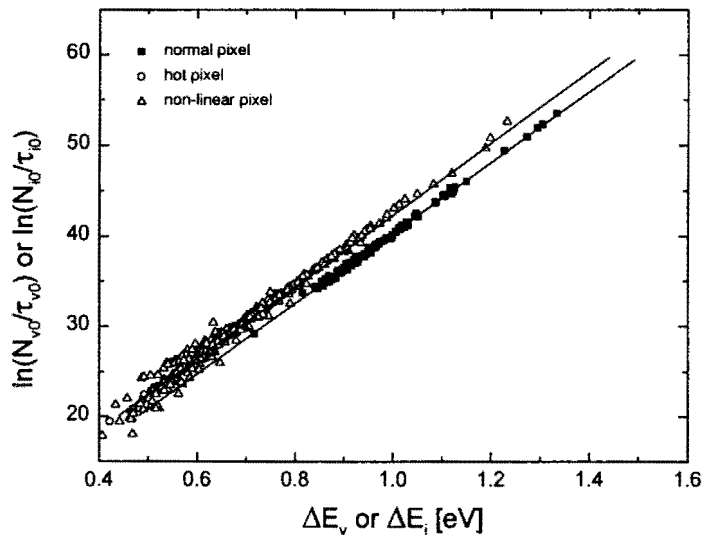
Fig. 46 Logarithm of the ratio N_{v0}/τ_{v0} or N_{i0}/τ_{i0} as a function of the activation energy. The results for normal pixels, hot pixels, and non-linear pixels are shown.

Figures 47 and 48 show the results for τ'_0 and $\Delta E'$. The analysis shows a wide spectrum in the activation energy.
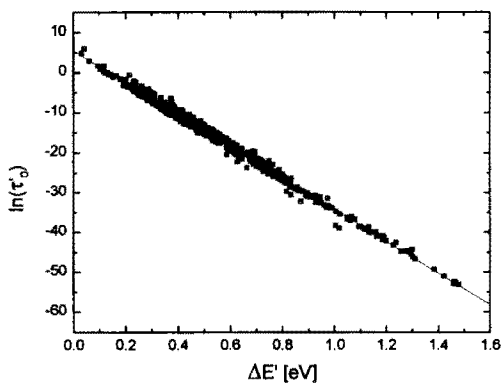
Fig. 47 Logarithm of τ'_0 as a function of the activation energy $\Delta E'$ for non-linear pixels.
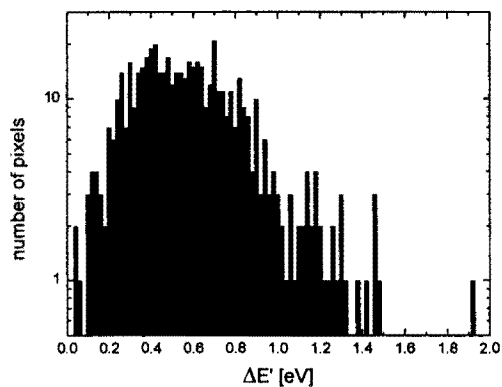
Fig. 48 Histogram of the activation energy for figure 47.

Finally, figures 49 and 50 show the result for $ln(N_{v0}/\tau_{v0})$ and the activation energy ΔE_{v0}. This part of the equation for non-linear pixels correspondends to the dark count caused from the bulk. An activation energy around 1.1 eV is expected.
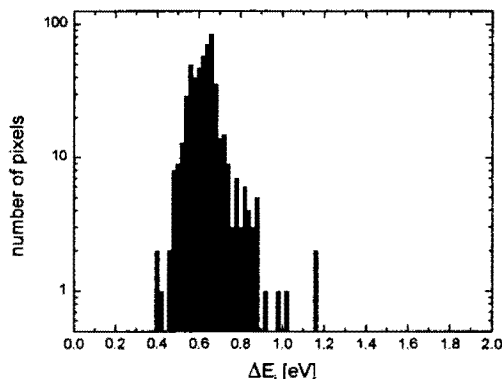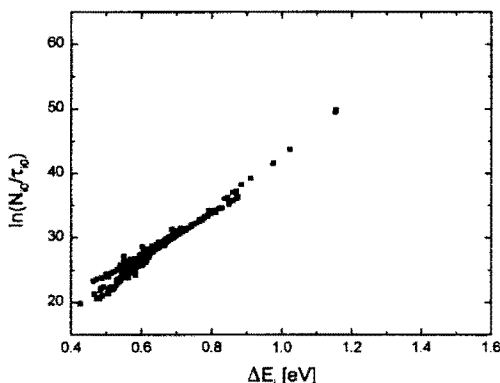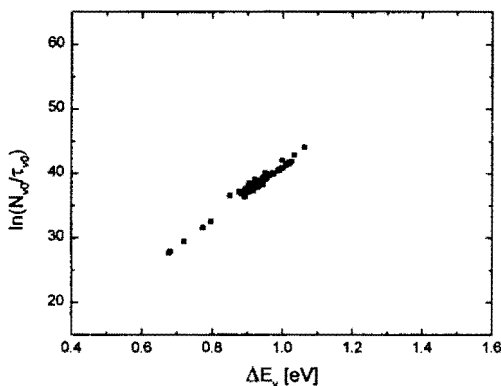

Fig. 49 Logarithm of the ratio N_{v0}/τ_{v0} as a function of the activation energy for non-linear pixels.
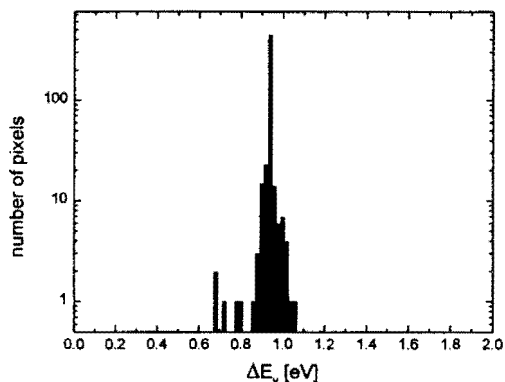
Fig. 50 Histogram of the activation energy for figure 49. The peak shows an activation energy of 0.95 eV.

Figure 50 shows that the peak for the activation energy is at 0.95 eV. This is in good agreement with the results for normal pixels. However, the difference from the results for normal pixels gives rise to an extended model which is discussed in appendix A.

In addition, figure 51 shows all results. It can be observed that $ln(N_{i0}/\tau_{i0})$ is proportional to the activation energy ΔE_{i0} and $ln(N_{v0}/\tau_{v0})$ is proportional to the activation energy ΔE_{v0}.
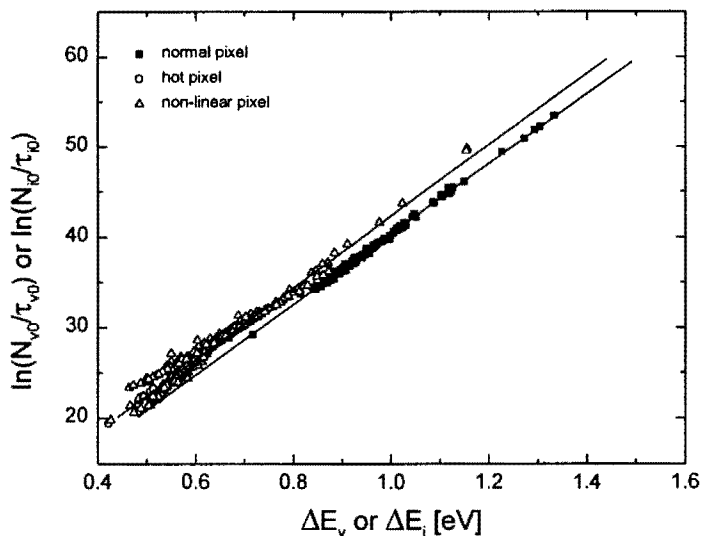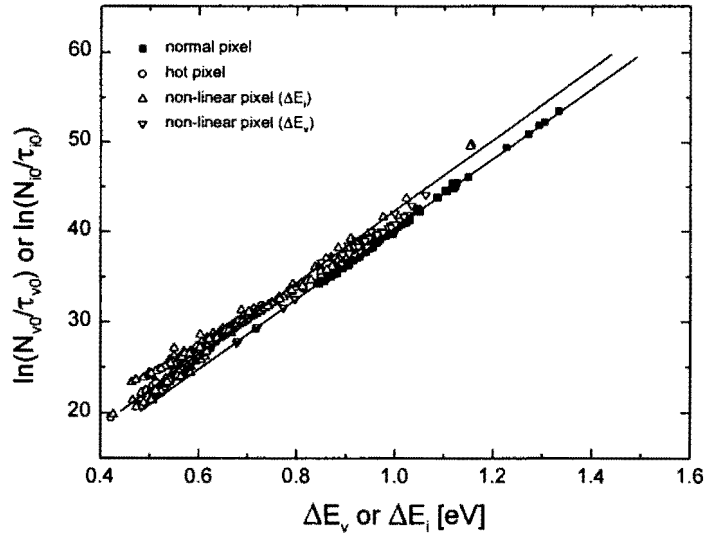
Fig. 51 Logarithm of the ratio N_{v0}/τ_{v0} or N_{i0}/τ_{i0} as a function of the activation energy. The results for normal pixels, hot pixels, and non-linear pixels are shown.

5.11 Meyer-Neldel rule

Many physical processes like thermally stimulated processes in polymers or electronic conduction in semiconductors obey the compensation law, or Meyer-Neldel rule.[21] This rule states that if a process X obeys the equation

$$X = X_0 \exp\left(\frac{-\Delta E}{kT}\right)$$

X_0 and ΔE obey the equation

$$\ln(X_0) = a + b * \Delta E$$

where a and b are constants. This can be observed in figure 47. $ln(\tau'_0)$ is proportional to $\Delta E'$ and can be written as

$$\ln(\tau_0) = MN_1 * \Delta E + MN_2$$

where MN_1 and MN_2 are the two Meyer-Neldel constants. The analysis of figure 47 gives the following parameters: MN_1=-39.7 and MN_2=5.45. This result can be used to calculate N_{v0} for normal pixels, N_{i0} for hot pixels, and N_{i0} for non-linear pixels of figures 36, 38, and 44. The following is for hot pixels. N_{i0} can be written as

$$\ln(N_{i0}) = \ln\left(\frac{N_{i0}}{\tau_{i0}}\right) + \ln(\tau_{i0})$$

where $\ln\left(\dfrac{N_{i0}}{\tau_{i0}}\right)$ are results from figure 38 and τ_{i0} can be expressed as

$$\ln(\tau_{i0}) = MN_1 * \Delta E_d + MN_2$$

This has been done for all pixels in the groups of normal pixels, hot pixels, and non-linear pixels. The results for the first one hundred randomly chosen pixels of each group are shown below. The results agree very well with the models described earlier. N_{v0} or N_{i0} is in all cases roughly constant and different for normal pixels compared to hot pixels respectively non-linear pixels.
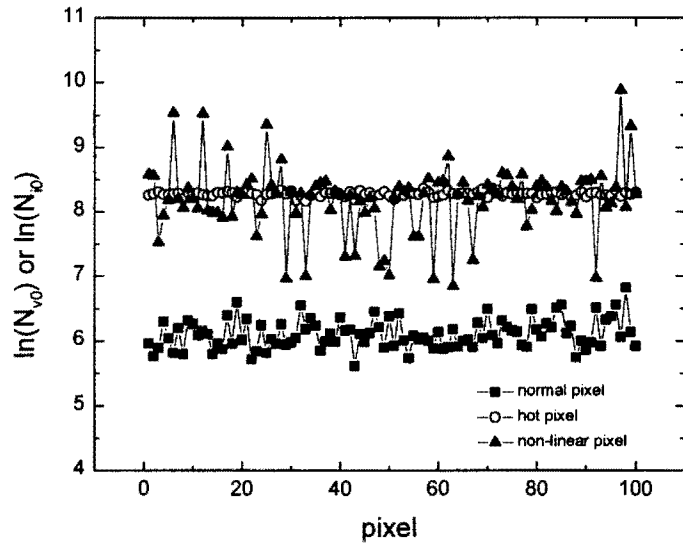
Fig. 52 *Ln(N$_{v0}$)* or *Ln(N$_{i0}$)* as a function of the ΔE_v or ΔE_i and τ_{v0} or τ_{i0} for the first one hundred randomly chosen pixels of the groups normal pixels, hot pixels, and non-linear pixels.

The following figure shows histograms for the calculation from above.
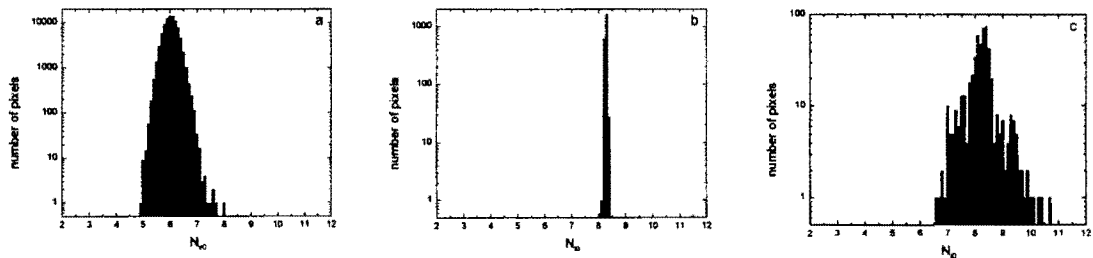
Fig. 53 *N$_{v0}$* respectively *N$_{i0}$* histograms. Figure a shows normal pixels, b hot pixels, and c non-linear pixels.

The results are: *ln(N$_{v0}$)*=6.09 for normal pixels, *ln(N$_{i0}$)*=8.27 for hot pixels, and *ln(N$_{i0}$)*=8.24 for non-linear pixels.

5.12 Conclusion

In this study the dark current of a CCD detector was examined in detail with a dark current characterization technique. A quantization of the dark current and the existence of different pixel groups in a CCD imager was shown. But more importantly, a group of pixels with a non-linear dark count behavior was identified.

The pixels were split into different groups (negative pixels, non-linear pixels, normal pixels, hot pixels) and models were developed to explain the different sources for the dark count. For each group an explanatory model and a statistical analysis technique have been developed which enables the derivation of the densities and the characteristic energies responsible for these effects. The fit between data and models is excellent. For normal pixels an activation energy of 1.05 eV was found. This is in good agreement with the diffusion current.[22] For hot pixels and non-linear pixels a second source of dark current was found to be responsible for the higher dark current. For this extra current an activation energy of 0.65 eV was determined. This is in good agreement with interface state generated dark current.

These dark counts are a source of unwanted signal (i.e., noise) in frames, and should be considered where very exact, low light-level signal processing is necessary. The techniques/analysis can also be used by manufacturers to gain important information regarding the nature of dark current and impurity states in CCD chips.

In addition, the compensation law or Meyer-Neldel rule was confirmed and used to calculate the number of filled impurity states for hot pixels and non-linear pixels.

6 Future work

In this thesis a systematic study of residual bulk images and a systematic study of dark current in a Kodak CCD imager were performed. In both studies explanatory models and statistical analysis techniques have been developed which enable the derivation of the densities and the characteristic energies responsible for these effects.

The effects are a source of unwanted signal in frames, and should be considered where very exact, low light-level signal processing is necessary. The techniques/analysis can also be used by manufacturers to gain important information regarding the nature of impurity states in CCD imagers.

For the systematic study of residual bulk images only a white light source was used. In extension to the described setup a repetition of the experiment with different wavelengths would give information about the location of impurity sites responsible for residual bulk images. For the systematic study of dark current a fit to the data with the model as described in appendix A could give more information. Furthermore the same experiments could be repeated with a back-illuminated CCD device.

7   Appendix A

In this appendix a slightly different model for non-linear pixels is described. In addition to the electrons thermally released from the valence band to the conduction band and the electrons thermally "hop" from the valence band into interface states and then to the conduction band it is assumed that also the impurity states get filled. The change in N_i can be written as

$$\frac{dN_i}{dt} = \frac{dN_c}{dt} + \frac{dN_r}{dt} + \frac{dN_f}{dt}$$

where dN_c/dt is the dark current rate thermally released from the impurity states to the conduction band, dN_r/dt is the rate thermally released from the impurity states, and dN_f/dt is the rate thermally released to the impurity states. It can be expected that dN_c/dt and dN_r/dt are proportional to N_i, the number of filled traps in the impurity states, and dN_v/dt should depend on the number of filled impurity states as well. This can be written as

$$\frac{dN_i}{dt} = -\frac{N_i}{\tau_i} - \frac{N_i}{\tau_r} + \frac{N_v}{\tau_f}\left(\frac{N_{max} - N_i}{N_{max}}\right)$$

$$\frac{dN_i}{dt} = -\frac{N_i}{\tau_i} - \frac{N_i}{\tau_r} - \frac{N_i}{\tau_f}\frac{N_v}{N_{max}} + \frac{N_v}{\tau_f}$$

$$\frac{dN_i}{dt} = -\frac{N_i}{\tau} + \frac{N_v}{\tau_f} = -\frac{N_i}{\tau} + c_1$$

with

$$\frac{1}{\tau} = \frac{1}{\tau_i} + \frac{1}{\tau_r} + \frac{1}{\tau_f}\frac{N_v}{N_{max}} \text{ , and } c_1 = \frac{N_v}{\tau_f}$$

where τ_i, τ_r , and τ_f are the characteristic time constants for the electrons and

can be written as

$$\tau_i = \tau_{i0}\exp\left(-\frac{\Delta E_i}{kT}\right), \ \tau_r = \tau_{r0}\exp\left(-\frac{\Delta E_r}{kT}\right), \ \tau_f = \tau_{f0}\exp\left(-\frac{\Delta E_f}{kT}\right)$$

Substituting

$$N_i = g_1(t)\exp\left(\frac{-t}{\tau}\right)$$

gives

76

$$c_1 = \frac{dN_i}{dt} + \frac{N_i}{\tau'} = -\frac{g_1}{\tau'}\exp\left(\frac{-t}{\tau'}\right) + \frac{dg_1}{dt}\exp\left(\frac{-t}{\tau'}\right) + \frac{g_1}{\tau'}\exp\left(\frac{-t}{\tau'}\right)$$

$$c_1 = \frac{dg_1}{dt}\exp\left(\frac{-t}{\tau'}\right)$$

$$dg_1 = c_1\exp\left(\frac{t}{\tau'}\right)dt$$

$$g_1 = c_1\tau'\exp\left(\frac{t}{\tau'}\right) + c_2$$

Thus, N_i can be written as

$$N_i = c_1\tau'\exp\left(\frac{t}{\tau'}\right)\exp\left(\frac{-t}{\tau'}\right) + c_2\exp\left(\frac{-t}{\tau'}\right) = c_2\exp\left(\frac{-t}{\tau'}\right) + c_1\tau'$$

with

$$N_i(0) = N_{i0} = c_2 + c_1\tau'$$

$$c_2 = N_{i0} - c_1\tau'$$

Combining this result with the dark current rate of thermal release from impurity states into the conduction band, dN_c/dt, can be written as

$$\frac{dN_c}{dt} = -\frac{N_i}{\tau_i} = -\frac{c_2}{\tau_i}\exp\left(\frac{-t}{\tau'}\right) - \frac{c_1}{\tau_i}\tau'$$

and the dark count from the impurity states is

$$I'(t) = \int_0^t \frac{c_2}{\tau_i}\exp\left(\frac{-t}{\tau'}\right) + \frac{c_1\tau'}{\tau_i}\,dt$$

$$I'(t) = -\frac{c_2}{\tau_i}\tau'\exp\left(\frac{-t}{\tau'}\right) + \frac{c_2}{\tau_i}\tau' + \frac{c_1}{\tau_i}\tau't$$

$$I'(t) = \frac{c_2}{\tau_i}\tau'\left(1 - \exp\left(\frac{-t}{\tau'}\right)\right) + \frac{c_1}{\tau_i}\tau't$$

Thus, using the equation for dN_v/dt from above, the dark count for non-linear pixels can be written as

$$I(t) = \frac{c_2}{\tau_i}\tau'\left(1 - \exp\left(\frac{-t}{\tau'}\right)\right) + \frac{c_1}{\tau_i}\tau't + \frac{N_v}{\tau_v}t$$

$$I(t) = \frac{c_2}{\tau_i} \tau' \left(1 - \exp\left(\frac{-t}{\tau'} \right) \right) + \left(\frac{c_1}{\tau_i} \tau' + \frac{N_v}{\tau_v} \right) t$$

where c_1, c_2, and τ' are

$$c_1 = \frac{N_v}{\tau_f}$$

$$c_2 = N_{i0} - \frac{N_v}{\tau_f} \tau'$$

$$\frac{1}{\tau'} = \frac{1}{\tau_i} + \frac{1}{\tau_r} + \frac{1}{\tau_f} \frac{N_v}{N_{max}}$$

8 References

[1] W.S. Boyle and G.E. Smith, Charge Coupled Semiconductor Devices, Bell Systems Technical Journal, vol. 49, pp. 587-593, April, 1970

[2] G.F. Amelio, M.F. Tompsett and G.E. Smith, Experimental Verification of the Charge Coupled Concept, Bell Systems Technical Journal, vol. 49, pp. 593-600, April, 1970

[3] W.E. Engeler, J.J. Tiemann and R.D. Baertsch, Surface Charge Transport in Silicon, Applied Physics Ltrs., 17, No. 11, p. 469, Dec. 1, 1970

[4] Scientific Imaging Technologie Inc. (SITe), An Introduction to Scientific Imaging Charge-Coupled Devices, 1996

[5] J. Janesick, T. Elliott, History and Advancements of Large Area Array Scientific CCD Imagers, Astronomical CCD Observing and Techniques, ASP Conference Series, vol. 23, 1992

[6] W.J. Toren, J. Bisschop, Complete Characterization of Dark Current in Frame Transfer Image Sensors, Philipps J. Res., vol. 48, pp. 207-231, 1994

[7] N.S. Saks, A Technique for Suppressing Dark Current Generated by Interface States in Buried Channel CCD Imagers, IEEE Electron Device Letters, Vol. EDL-1, No. 7, July 1980

[8] J. Bosier, FT-CCD for Consumer Applications with Low Dark Current by Surface Pinning, Phillips J. Res., vol 48, 1994

[9] J. Janesick, CCD Transfer Methods – Standard for Absolute Performance of CCDs and Digital CCD Camera Systems, 1992

[10] Axiom Research Inc., AX Series CCD Camera User's Guide, Version 1.0 Rev. D, June 1995

[11] A. Rest, Calibration of a CCD camera and correction of its images, Master thesis, Physics Department, Portland State University, August 1996

[12] N. S. Saks, Interface state trapping and dark current generation in buried-channel charge-coupled devices, J. Appl. Phys., vol. 53(3), March 1992

[13] W. J. Toren, J. Bisschop, Improved Charge-Transfer Inefficiency Methods for Determining Ultra Low Concentrations of Bulk States in Charge-Coupled Devices, Philipps J. Res. 48, pp. 197-206, 1994

[14] P. M. Epperson, Electro-optical characterization of the Tektronix TK512M-011 charge-coupled device, Optical Engineering, vol. 26 No. 8, pp. 715-724, 1987

[15] J. Janesick, T. Elliott, History and Advancements of Large Area Array Scientific CCD Imagers, Astronomical CCD Observing and Techniques, ASP Conference Series, vol. 23, 1992

[16] R.L. Gilliland, Details of Noise Sources and Reduction Processes, Astronomical CCD Observing and Reduction Techniques, ASP Conference Series, vol. 23, 1992

[17] R.D. McGraph, J. Doty, G. Lupino, G. Ricker, and J. Vallerga, Counting of deep-level traps using a charge-coupled device, IEEE Trans. Eletron Devices, vol. ED-34, pp.2555-2557, 1987

[18] W.C. McColgin, J.P. Lavine, J. Kyan, D.N. Nichols, and C.V. Stancampiano, Dark current quantization in CCD Image Sensors, International Electron Device Meeting 1992, p. 113, 13-16 Dec. 1992

[19] N.S. Saks, A Technique for Suppressing Dark Current Generated by Interface States in Buried Channel CCD Imagers, IEEE Electron Device Letters, Vol. EDL-1, No. 7, July 1980

[20] W. Meyer, H. Neldel, Z. Tech. Phys. 12, 588, 1937

[21] K.L. Narasimham, B.M. Arora, The Capture of Cross-Section and the Meyer-Neldel Rule in III-V Compound Semiconductors, Solid State Communications, Vol. 55, No. 7, pp. 615-617, 1985

[22] A.S. Grove and D.J. Fitzgerald, Solid-State Electron. 9, 783, 1966